PYRAZOLYL BASED LIGANDS IN TRANSITION METAL COMPLEXES

by

MICHAEL DAVID OLSON

B.SC., UNIVERSITY OF BRITISH COLUMBIA, 1986

A THESIS SUBMITTED IN PARTIAL FULFILLMENT OF

THE REQUIREMENT FOR THE DEGREE OF

MASTER OF SCIENCE

in

THE FACULTY OF GRADUATE STUDIES

DEPARTMENT OF CHEMISTRY

We accept this thesis as conforming

to the required standard

THE UNIVERSITY OF BRITISH COLUMBIA

SEPTEMBER, 1989

In presenting this thesis in partial fulfilment of the requirements for an advanced degree at the University of British Columbia, I agree that the Library shall make it freely available for reference and study. I further agree that permission for extensive copying of this thesis for scholarly purposes may be granted by the head of my department or by his or her representatives. It is understood that copying or publication of this thesis for financial gain shall not be allowed without my written permission.

Department of Chemistry

The University of British Columbia
Vancouver, Canada

Date Sept 28/89

DE-6 (2/88)

Abstract

Several uninegative, multidentate pyrazolyl based ligands were synthesized [eg. $HBpz_3^-$, $HBpz"_3^-$, $MeGapz_3^-$, $MeGapz"_3^-$, $H_2Bpz_2^-$, $Me_2Bpz_2^-$, $Me_2Gapz_2^-$, $Me_2Gapz"_2^-$, $Me_2Gapz(OCH_2CH_2NH_2)^-$, $Me_2Gapz(OCH_2CH_2CH=CH_2)^-$; pz = pyrazolyl, pz" = 3, 5 dimethylpyrazolyl].

These ligands were reacted with the sterically hindered metal complex, $HBpz^*_3MCl$ (M = Co, Ni; pz* = 3-iPr-4-Br-pyrazolyl) and the mixed-ligand transition metal complexes of general formulae, $HBpz^*_3ML$, were isolated. The X-ray crystal structure of one such complex, $HBpz^*_3Nipz"_3BH$ was determined showing a near octahedral arrangement of ligands about the nickel centre. The electronic spectra of the nickel complexes were recorded and compared to predicted transitions. The electronic spectra of the four coordinate nickel complex, $HBpz^*_3NiCl$, fit a d^8, tetrahedral, ligand field model. The six coordinate complexes, $HBpz^*_3NiL$ (L = $HBpz_3$, $HBpz"_3$, $MeGapz_3$, $MeGapz"_3$), fit a d^8, octahedral, ligand field model.

The unsymmetrical pyrazolylgallate ligands were reacted with the rhodium dimer $[Rh(CO)_2Cl]_2$ to give the square planar complexes, $LRh(CO)$ [L = $Me_2Gapz(OCH_2CH_2NH_2)$, $Me_2Gapz(OCH_2CH_2CH=CH_2)$]. These rhodium[I] complexes appeared to undergo oxidative additions of MeI, allylbromide and I_2. Furthermore these rhodium[I] complexes appeared to bind the

small gas molecules, CO and ethene.

A number of heterobimetallic complexes, with direct metal-metal bonds, were prepared and isolated from the reaction of the molybdenum anion, $HBpz''_3(CO)_3Mo^-$ with the transition metal halides, $[CuPPh_3Cl]_4$, SnR_3Cl (R = Me, Ph) and $GePh_3Cl$.

Table of Contents

List of Tables

List of Figures

List of Abbreviations

The following abbreviations have been used in this thesis.

A	Angstrom
amu	atomic mass unit
B	Racah parameter
B.M.	Bohr Magneton
but	but-3-enolate
^{o}C	degree Celsius
calc.	calculated
cf	confer (Latin : compare)
cm^{-1}	reciprocal centimeters (wave numbers)
Co.	company
C.T.	charge transfer band
EA	ethanolamino
Fig.	figure
g	grams
g	gerade
Hpz	pyrazole
i.e.	id est (Latin : that is)
iPr	isopropyl
IR	infrared
L	pyrazolyl based ligand
M	transition metal
m/e	mass to charge ratio
Me	methyl

ml	millilitres
mmole	millimoles
nm	nanometers
No.	number
O_h	octahedral
P	parent (peak)
Ph	phenyl
pz	pyrazolyl
pz"	3,5-dimethylpyrazolyl
pz*	3-isopropyl-4-bromo-pyrazolyl
t-bu	tertiary butyl
T_d	tetrahedral
10 D_q	crystal field splitting energy
THF	tetrahydofuran
tren	triethylamino amine
u	ungerade
U.B.C.	University of British Columbia
UV	ultraviolet
Vis	visible
Vol.	Volume
E	extinction coefficient
n	hapto (Greek, haptein : to fasten)
n^3	trihapto
n^5	pentahapto
π	pi
u_B	magnetic moment
$,^,#,@	footnote markers

Acknowledgement

I would like to express my sincere thanks to Dr. Alan Storr for his guidance, wisdom and wit that made this project a stimulating 2 years of research. I extend my thanks to my very good friends Tammy, Martin, Gord and Jane for their help and tolerance.

My thanks to the Faculty and technical staff at U.B.C., in particular Peter Borda and Steve Rettig for their dedication to excellence.

Financial support from U.B.C. Teaching Assistantship is gratefully acknowledged.

Chapter I

Polypyrazolyl Based Ligands in Transition Metal Complexes

1.1 General Introduction

The viability of the polypyrazolylborates as a ligand system began with their discovery in 1966 by S. Trofimenko[1]. Since then several reviews[1,2,3,4] and the numerous publications referenced therein have demonstrated the unique characteristics and versatility of these ligands.

Pyrazole is a five membered heterocyclic compound (Fig. 1.1) that will react with certain compounds containing main group elements, forming multidentate, uninegative ligands.

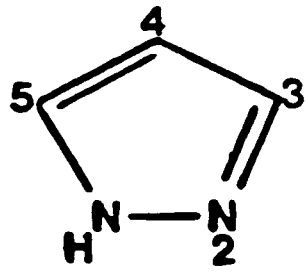

Figure 1.1 Pyrazole

In particular the polypyrazolylborate ligands are of the general formula $[R_nBpz_{4-n}]^-$ (pz = pyrazolyl; n = 0-2; R = H, alkyl, aryl) and can function as bidentate ligands (n = 0-2) or as tridentate ligands (n = 0,1) (Fig. 1.2).

Figure 1.2 Polypyrazolylborate Ligands

Symmetrical Bidentate

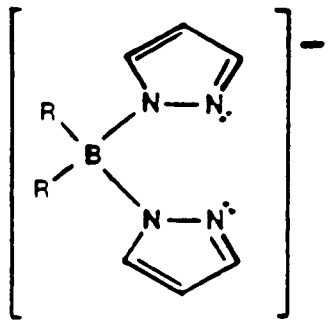

R_2Bpz_2

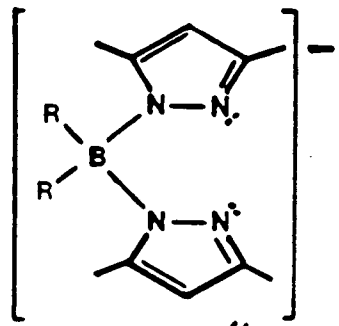

$R_2Bpz''_2$

Symmetrical Tridentate

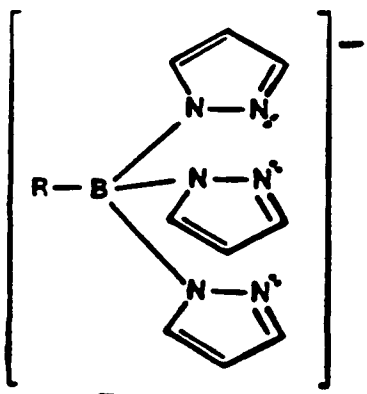

$RBpz_3$

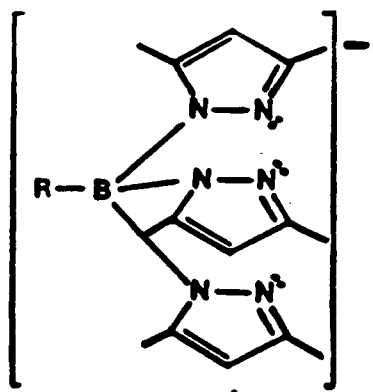

$RBpz''_3$

These ligands generally form bis-ligand complexes with first-row divalent transition metals[5,6].

The tridentate ligands are uninegative six electron donors and bond to the metal through the three nitrogen lone pairs in a tripodal fashion.

The bidentate ligands are uninegative four electron donors that form a six member ring on coordination with the metal centre. A boat shaped (or planar) conformation is forced on the structure by the constraint that both the boron and metal must be simultaneously coplanar with each pyrazolyl ring to retain the resonance stabilization energy in each pyrazolyl ring[3].

The versatility of the ligand system comes through the numerous substitutional possibilities that provide means of imparting steric and electronic control about the metal centre. Substitutions can be made on the pyrazolyl ring, the terminal group on the boron atom can be altered and the boron atom itself can be replaced. An example is a steric stabilizing effect brought about by methyl substitution on the pyrazolyl ring[1,7]. For example, $(H_2Bpz_2)_2Fe$ is air-sensitive but $(H_2Bpz"_2)_2Fe$ (pz" = 3,5-dimethylpyrazolyl) is air-stable. It is suggested that the methyl group in the 3 position covers the metal center, protecting it from nucleophilic attack.

Bulkier substituents at the 3 position of the pyrazolyl ring can lead to the formation of mono-ligand complexes of the divalent metals[8]. For example placing a tertiary butyl

group in the 3 position gives the mono-ligand chloride complex, $HB(3\text{-t-bu-pyrazolyl})_3MCl$ (M = Co)[7].

Displacement of the halide from these mono ligand complexes leaves a sterically and electronically controlled active pocket. In chapter two of this work the pocket of one such mono ligand complex is examined by reactions with less sterically demanding ligands and a mixed-ligand transition metal series is developed.

Electronic effects brought about by the ligand systems have been demonstrated by substitutions on the pyrazolyl ring or varying the terminal group. An example of this effect is seen in the magnetic behaviour of a series of iron[II] complexes (at room temperature)[2].

	u_B (B.M.)	
$[pzBpz_3]_2Fe$	0.0	diamagnetic
$[HBpz_3]_2Fe$	2.71	temperature dependent paramagnetism
$[HBpz"_3]_2Fe$	5.03	paramagnetic

Iron[II] in a d^6 octahedral complex and would have four free electrons in a high spin structure. A low spin structure would have all electrons paired and therefore be diamagnetic.

The magnetic behaviour of these complexes is a result of substitutions on the pyrazolyl ligand. The $[pzBpz_3]^-$ ligand is a stronger field ligand than is $[HBpz_3]^-$ as seen by the magnetic moments (u_B) of their iron[II] complexes.

The fourth pyrazolyl ring contributes electron density toward the metal bonding orbitals of the $[pzBpz_3]^-$ ligand (inductive effect). This enhanced sigma donating ability of the $[pzBpz_3]^-$ ligand is great enough to force the pairing of all the iron[II] electrons and thus form a low spin complex.

The $[HBpz_3]^-$ ligand is a stronger field ligand than is the $[HBpz"_3]^-$ ligand as seen above by the magnetic moments of their iron[II] complexes. This is an example of where electronic effects and steric effects can be at odds with each other. Methyl substitution on a pyrazolyl ring would make the ring more basic by electron donation of the methyl groups (inductive effect). The substituted ring would then become a better sigma donor toward a metal centre and thus a stronger field ligand. The reverse effect is seen in comparing the magnetic moments of $[HBpz_3]_2Fe$ and $[HBpz"_3]_2Fe$. It is likely that steric crowding of the methyl groups of the $[HBpz"_3]^-$ ligand causes the ligand to coordinate the iron centre at a greater distance than the $[HBpz_3]^-$ ligand, thus forming the high spin complex. This makes the $[HBpz"_3]^-$ ligand a weaker field ligand than $[HBpz_3]^-$ for steric reasons.

A further example of this conflict of electronic and steric factors is the reaction of the $[MeGapz"_3]^-$ ligand (borate analogue) with divalent transition metals. The enhanced sigma donating ability brought about by the methyl substituents is sometimes outweighed by the steric interactions of the methyl groups on attempted complexation.

Often the ligand will not form tris-chelated complexes with the divalent transition metals, instead the ligand fragments and forms a dimer complex where the substituted pyrazolyl rings bridge between metal atoms[9,10].

Analogues of the pyrazolylborates have been made by replacement of the boron atom with a gallium atom (Fig. 1.3). The difference in electronegativities (Allred-Rochow) of gallium (1.82) and boron (2.01) make the gallate ligands better sigma donors which is evidenced by IR measurements of analogous carbonyl complexes[11].

An unsymmetrical pyrazolylgallate ligand system has been recently developed (Fig. 1.3) that has demonstrated unique coordination behaviour in that it may coordinate to a metal centre in either a facial or meridional manner[12]. Furthermore these ligands have shown some promise in forming square planar rhodium[I] complexes that may have catalytic activity. These ligands and their rhodium[I] complexes are described in chapter three. The reactivities of these complexes are also described.

The tris chelating pyrazolylborate and pyrazolylgallate ligands have been used to form the anionic complex $[LMo(CO)_3]^-$ (L = $MeGapz_3$, $HBpz_3$, $HBpz"_3$). These molybdenum anionic complexes have been reacted with transition-metal halides to form heterobimetallic compounds with direct metal-metal bonds. The fourth chapter describes the synthesis of several new heterobimetallic complexes incorporating the molybdenum anion, $[HBpz"_3Mo(CO)_3]^-$.

1.2 General Techniques

Air sensitive materials were handled in a dry box (Vacuum Atmospheres Corporation). Reactions where carried out in the dry box or under a nitrogen atmosphere.

The solvents were dried by refluxing with an appropriate drying agent and collected by distillation under a nitrogen blanket. The solvents THF and hexane were refluxed with sodium metal, using benzophenone as an indicator. Benzene was refluxed with potassium metal. Methylene chloride was refluxed with calcium sulphate. Methylcyanide was refluxed with phosphorous pentoxide (P_2O_5). The distilled solvents were stored in the dry box under nitrogen.

A vacuum line fitted with a Duo Seal Vacuum Pump was routinely used to dry samples and when fitted with a liquid nitrogen cooled solvent trap was used to remove solvents from reaction mixtures.

Infrared spectra were recorded using a Perkin Elmer 598 spectrometer and were calibrated using the 1601 cm^{-1} band of a polystyrene standard. Infrared spectra where recorded using KBr solution cells with a reference cell containing a solvent blank or using Nujol mulls spread between KBr windows.

Microanalyses were performed by Mr. Peter Borda of the U.B.C. Microanalytical Services using a Carlo Erba Elemental Analyser.

Mass spectra were recorded by the U.B.C. Mass Spectrometry Services using a Kratos MS50 mass spectrometer. Ionization of compounds was done by electron impact.

X-ray stuctures were determined by Dr. S.J. Rettig of this department using a Rigaku single crystal X-ray diffractometer.

UV/Vis spectra were recorded with a Shimadzu UV-2100 spectrometer and near-infrared spectra with a Cary 14 spectrometer.

Figure 1.3 Polypyrazolylgallate Ligands

Symmetrical Bidentate

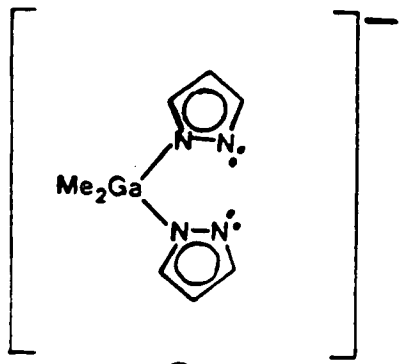

Me_2Gapz_2

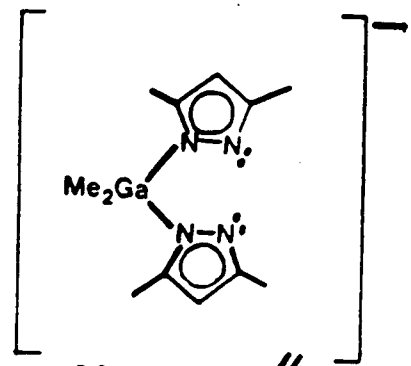

$Me_2Gapz''_2$

Symmetrical Tridentate

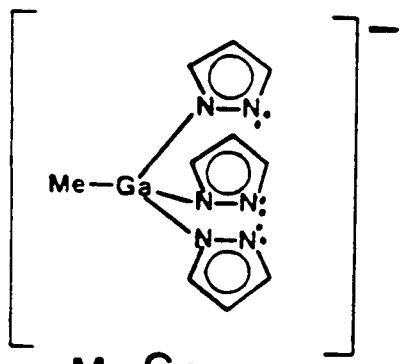

$MeGapz_3$

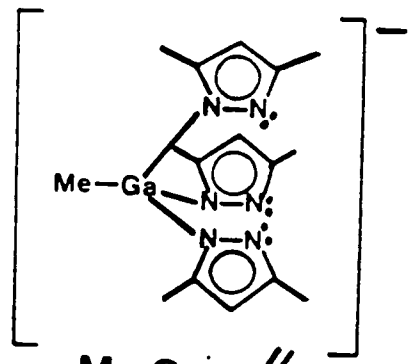

$MeGapz''_3$

Unsymmetrical Tridentate

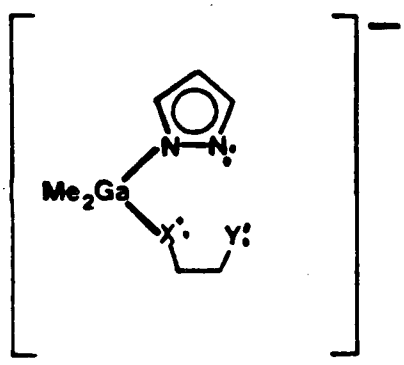

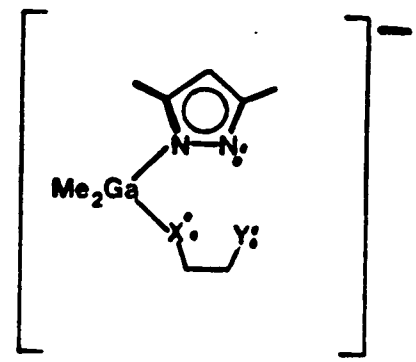

Chapter II

Mixed Ligand Complexes

2.1 Introduction

One of the basic precepts in designing a ligand system is to impart steric and electronic properties to the reactive site of the transition metal such that it may produce selective and consistent reactivity.

The ultimate manifestation of this principle is demonstrated to us by the reactive sites on enzymes. These sites are very nearly perfect in their selectivity and reactivity to a particular substrate. This is accomplished by the enzyme through ideal steric and nucleophilic conditions and subtle conformational changes in the surrounding organo-mass. Mimicking these selective pockets is one of the goals of organometallic chemistry.

The discovery of new and more intricate tris-chelating pyrazolylborates is providing new inroads into this type of chemistry.

In these ligand systems the 3 position on the pyrazolyl ring is the most sterically influential site about the metal center (Fig. 2.1). Ligands with H or Me in this position readily form bis-ligand complexes with divalent transition metals. However, when a bulky group such as the tertiary

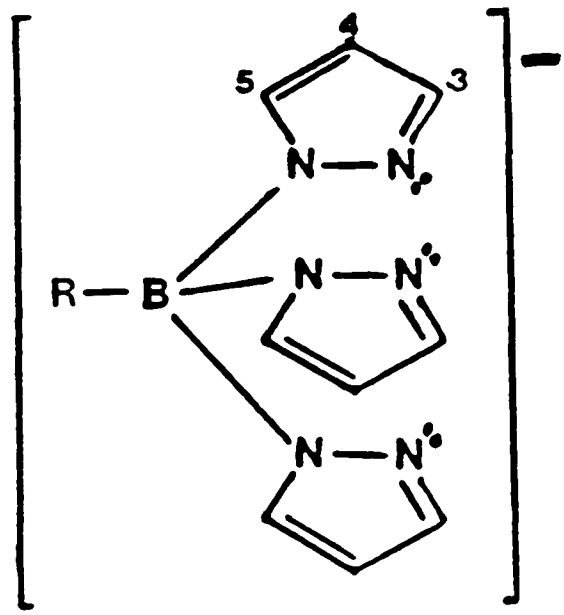

Figure 2.1 Tris-chelating Pyrazolylborate Ligand

butyl group is in the 3 position only the mono ligand complex will form. Presumably this is due to steric hinderance by the tertiary butyl group around the metal[13].

Trofimenko has designed, what he has called, intermediate ligands by placing an isopropyl group in the 3 position. These ligands are sterically restricted, but form a bis-ligand complex with a peculiar 1,2 borotropic shift[14].

$$2\ HB(3\text{-}iPrpz)_3^- + Co^{2+} \rightarrow [HB(3\text{-}iPrpz)_2\ (5\text{-}iPrpz)]_2Co$$

This rearrangement of the pyrazolyl rings suggests that the intermediate ligand has created a sterically controlled active pocket around the metal centre.

In an effort to examine the active pocket created by

the intermediate ligand $[HBpz^*_3]^-$ (pz^* = 3-iPr-4Br-pyrazolyl) the complex $HBpz^*_3MCl$ (Fig. 2.2) was reacted with sterically smaller pyrazolylborate and pyrazolylgallate ligands (Fig. 1.2, 1.3) to produce a series of mixed-ligand metal complexes.

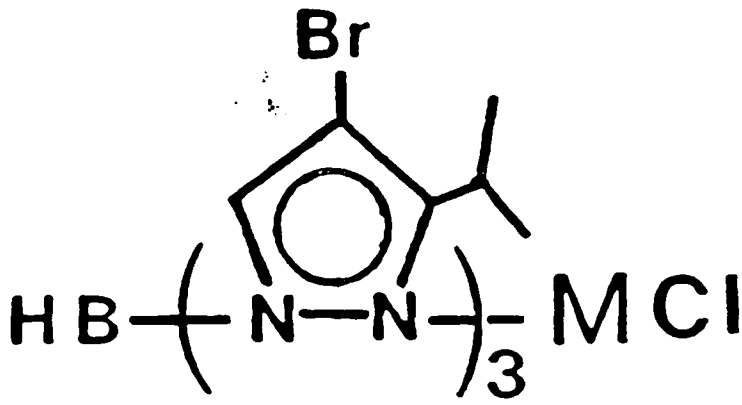

Figure 2.2 $HBpz^*_3MCl$ (M = Co, Ni)

In this chapter the syntheses of the smaller pyrazolyl based ligands, the syntheses of the mixed-ligand metal complexes and the characterizations of these complexes is described. The series includes 4, 5 and 6 coordinate mixed-ligand metal complexes and representative complexes from each coordination mode are given as examples in the characterization studies. The complete series is listed in Tables 2.1.a and 2.1.b on pages 22 and 23..

A UV/Vis study was performed on the mixed-ligand nickel series to further characterize the complexes. The transition

energies calculated from the recorded spectra were compared with predicted energies from high symmetry models for each particular coordination number.

2.2 Experimental

2.2.1 Starting Materials

Pyrazole (Hpz) and 3,5-dimethylpyrazole (Hpz") were obtained from K and K Laboratories and were used as supplied without further purification.

Literature methods were used to prepare Me_3Ga[15], $MeGaCl_2$[16] and Napz[17].

The bulky ligand metal complexes, HB(3-iPr-4Br-pyrazolyl)$_3$ MCl (M = Ni,Co) were supplied by S. Trofimenko. The complexes were prepared by reacting an excess of the metal chloride with the borate ligand[14]. A crystal structure of the cobalt complex was determined.

2.2.2 Syntheses of Bidentate Ligands

2.2.2a Preparation of $K^+[H_2Bpz_2]^-$ [18]

$$K^+BH_4^- + 2\ Hpz \xrightarrow[102\ ^oC]{-----} K^+[H_2Bpz_2]^- + 2\ H_2$$

This ligand was previously prepared by the above scheme. The extent of pyrazole incorporation is dependent on the temperature of the reaction as seen below (Fig. 2.3.).

The poly(1-pyrazolyl) borates are all air-stable and moisture-stable, white solids.

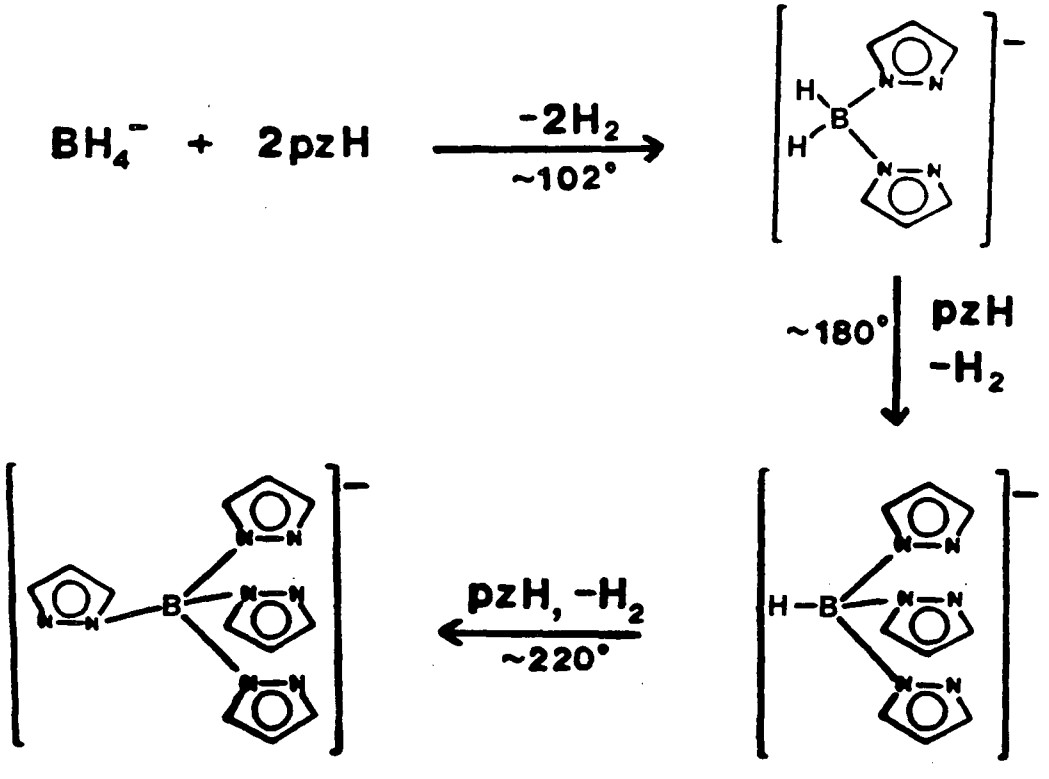

Figure 2.3 Preparation of Poly(1-pyrazolyl) Borate Ligands

2.2.2b Preparation of $Na^+[Me_2Bpz_2]^-$ [6]

$$Me_3B + Napz \longrightarrow Na^+[Me_3Bpz]^-$$

$$Na^+[Me_3Bpz]^- + Hpz \longrightarrow Na^+[Me_2Bpz_2]^- + MeH$$

This compound had been previously prepared by the above scheme. Quantities required were weighed out and dissolved in THF.

2.2.2c Preparation of $Na^+[Me_2Ga(pz)_2]^-$ and $Na^+[Me_2Ga(pz")_2]^-$ [6]

$$NaH + Hpz \longrightarrow Napz + H_2$$

$$Me_3Ga + Napz \longrightarrow Na^+ [Me_3Gapz]^-$$

$$Na^+ [Me_3Gapz]^- + Hpz \longrightarrow Na^+[Me_2Gapz_2]^- + MeH$$

To 150 ml of THF in a round bottom flask were added molar equivalents of $GaMe_3$ (1.510 g; 13.17 mmole) and Napz (1.185 g; 13.17 mmole). The mixture was stirred overnight. The resulting solution was made up to a known volume with THF and stored under a nitrogen atmosphere.

A 25 ml aliquot of the solution of $Na^+[Me_3Gapz]^-$ (2.63 mmole) was mixed with a 1:1 molar ratio of Hpz (0.179 g; 2.63 mmole) and refluxed under a nitrogen atmosphere. The

reaction proceeded with the evolution of methane and was monitored by the disappearance of the pyrazole N-H stretch at 3300 cm^{-1} in the IR spectrum. The mixture was then made up to a known volume with THF.

$[Me_2Gapz"_2]^-$ was prepared in a like manner. An aliquot of $Na^+[Me_3Gapz"]^-$ was mixed with a 1:1 stoichiometric amount of 3,5-dimethyl pyrazole (0.533 g; 5.55 mmole) and refluxed under nitrogen. On completion of the reaction the mixture was made up to a known volume with THF.

2.2.3 Syntheses of Symmetrical Tridentate Ligands

2.2.3a Preparation of $K^+[HBpz_3]^-$ and $K^+[HBpz"_3]^-$ [7]

$$K^+BH_4^- + 3\ Hpz \xrightarrow[180\ ^oC]{} K^+[HBpz_3]^- + 3\ H_2$$

This ligand and the tris (3,5-dimethylpyrazolyl) analog were previously prepared by the above scheme. The temperature of reaction determines the number of pyrazolyl rings bonding to the boron atom (Fig. 2.3)

2.2.3b Preparation of $Na^+[MeGapz_3]^-$ and $Na^+[MeGapz"_3]^-$[11]

$$MeGaCl_2 + 3\ Napz \longrightarrow Na^+[MeGapz_3]^- + 2\ NaCl$$

A molar equivalent of $MeGaCl_2$ (2.28 mmole) in THF, was added to a 3 molar equivalent of Napz (1.85 g; 6.85 mmole) dissolved in 30 ml of THF. The reaction mixture was stirred for one week under a nitrogen atmosphere. The resulting solution was made up to a known volume by addition of THF.

The 3,5-dimethylpyrazolyl analog was prepared in a similar manner by the reaction of three molar equivalents of Napz" (0.971 g; 2.74 mmole) with a molar equivalent of $MeGaCl_2$ (0.913 mmole). Both ligands were stored as solutions under a nitrogen atmosphere.

The alkali metal salts of the poly(1-pyrazolyl) gallate anions can be isolated as white solids but are hygroscopic (unlike the borate analogues).

2.2.4 Syntheses of Unsymmetrical Gallate Ligands

2.2.4a Preparation of $Na^+[Me_2Gapz(OCH_2CH_2NH_2)]^-$ [12]

$$Na^+[Me_3Gapz]^- + HOCH_2CH_2NH_2 \xrightarrow[\text{reflux}]{} Na^+[Me_2Gapz(OCH_2CH_2NH_2)]^- + MeH$$

To a THF solution of $Na^+[Me_3Gapz]^-$ (5.10 mmole) was added a molar equivalent of ethanolamine (0.311 g; 5.10 mmole). The mixture was refluxed for 40 hours until the O-H stretch of the alcohol at 3480 cm^{-1} in the IR spectrum disappeared. A peak at 570 cm^{-1} which grew during the course of the reaction was attributed to a Ga-O stretch and provided a good monitor for the reaction progress as well (Fig.2.4). The resultant mixture was then made up to a known volume by addition of THF and stored under a nitrogen blanket.

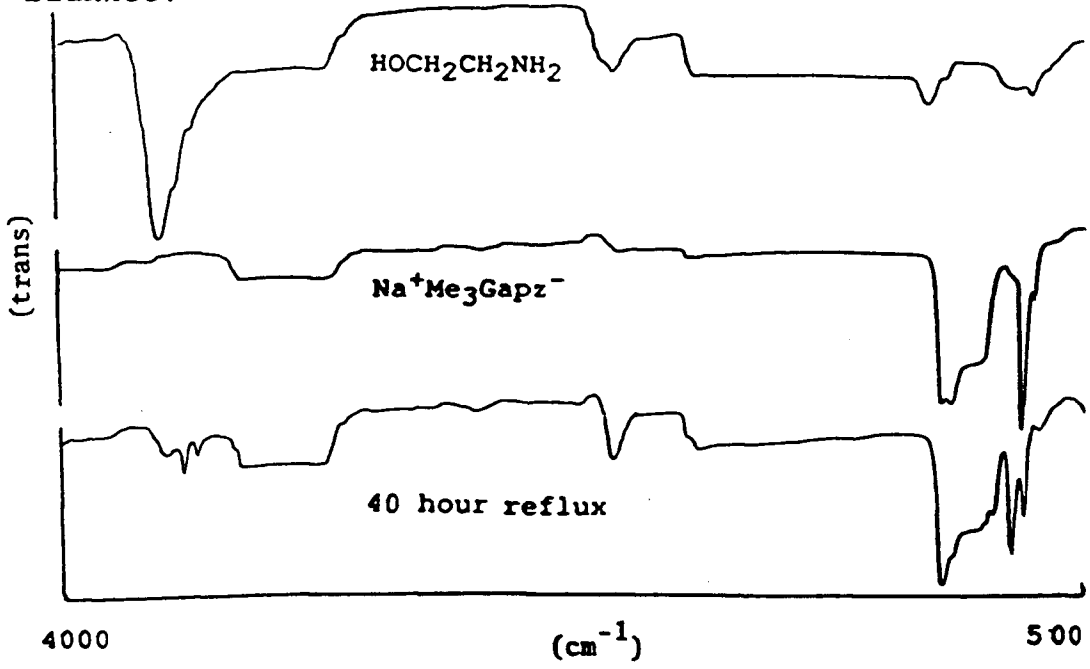

Figure 2.4 IR Spectra of $HOCH_2CH_2NH_2$, $Na^+[Me_3Gapz]^-$ and $Na^+Me_2Gapz(OCH_2CH_2NH_2)^-$

2.2.4b Preparation of $Na^+[Me_2Gapz(OCH_2CH_2CH=CH_2)]^-$ [19]

$$Na^+[Me_3Gapz]^- \quad \text{----->} \quad Na^+[Me_2Gapz(OCH_2CH_2CH=CH_2)]^-$$
$$+ HOCH_2CH_2CH=CH_2 \quad \text{reflux} \quad + MeH$$

To a THF solution of $Na^+[Me_3Gapz]^-$ (5.10 mmoles) was added a molar equivalent of but-3-enol (0.368 g; 5.10 mmoles) and the mixture was refluxed for 40 hours. The reaction was complete when the O-H stretch of the alcohol at 3470 cm^{-1} in the IR spectrum disappeared. The solution was then made up to a known volume with THF and stored under a nitrogen blanket.

2.2.4c Preparation of $Na^+[Me_2Gapz"(OCH_2CH_2NH_2)]^-$

$$Me_3Ga + Napz" \quad \text{--->} \quad Na^+[Me_3Gapz"]^-$$

$$Na^+[Me_3Gapz"]^- + HOCH_2CH_2NH_2 \text{ ---> } Na^+[Me_2Gapz"(OCH_2CH_2NH_2)]^-$$
$$\text{reflux} \quad + MeH$$

To a THF solution of Me_3Ga (27.8 mmole) was added a molar equivalent of Napz" (3.28 g; 27.8 mmole). This mixture was stirred overnight and then made up to a known volume by the addition of THF.

A 50 ml aliquot of this solution was reacted with a molar equivalent of ethanolamine and refluxed for 24 hours. The loss of the O-H band of the alcohol in the IR spectrum

signalled the completion of the reaction. This mixture was then made up to a known volume with THF.

2.2.5 Syntheses of Mixed-Ligand Metal Complexes

$$HBpz^*_3MCl + NaL \longrightarrow HBpz^*_3ML + NaCl$$

(M = Ni, Co; pz* = 3-iPr-4Br-pyrazolyl)

[L = $HBpz_3$, $HBpz"_3$, $MeGapz_3$, $MeGapz"_3$, H_2Bpz_2, Me_2Bpz_2, Me_2Gapz_2, $Me_2Gapz"_2$, $Me_2Gapz(OCH_2CH_2NH_2)$, $Me_2Gapz(OCH_2CH_2CH{=}CH_2)$]

The general reaction procedure was to place an aliquot of a THF solution of the less sterically bulky ligand (NaL) into a round bottom flask and begin stirring. A molar equivalent of the bulky ligand metal chloride complex ($HBpz^*_3MCl$) dissolved in THF was then added dropwise. The solution was stirred for a minimum of 24 hours under a nitrogen atmosphere. The reaction solvent (THF) was then removed under vacuum to a cold trap.

The following procedures were used until a satisfactory microanalysis was obtained.

1) The reaction product was redissolved in benzene and the mixture filtered. The benzene was allowed to evaporate slowly to promote crystal growth.

2) The reaction product was redissolved in 30 ml methylene chloride, filtered and 15 ml of hexane was added. The

solvent was evaporated slowly to promote crystal growth.

3) The reaction product was dried under vacuum at 70 ^{o}C.

4) The reaction product was sublimed. Most complexes appeared to be quite robust and sublimed at 220-250 ^{o}C under vacuum, but there were impurities that also sublimed.

5) A solvent extraction with 50:50 methylene chloride/water was performed on the reaction product. Three washings would be done and the compound would then be dried on the vacuum line at 70 ^{o}C. This method seemed to give the most satisfactory results and it is recommended for future work that this be the first method tried.

6) The reaction product was placed in a crystal grower. The crystal grower is shown in appendix 1. The compound was placed in one of the tubes and the apparatus attached to the vacuum line. The grower was evacuated and methylene chloride (or any other suitable solvent) was condensed into the tube. The tube was then flame sealed at the constriction nearest the vacuum line attachment thus making a sealed crystal growth environment. The concentration of solute could be controlled by condensing solvent into the other finger. If crystals grew the solvent would be decanted into this same finger. The crystals would be removed by freezing the solvent, flame sealing at the next constriction and removal to the glove box.

Pertinent data of the mixed-ligand metal complexes is collected in Tables 2.1.a and 2.1.b and the purification method that gave satisfactory analysis is indicated.

Table 2.1.a Analytical Data of $HBpz^*_3ML$
(L = mono- and tris-chelating ligands)

L	Metal	Color	Mass[$] (amu)	Microanalyses C	H	N	Purification Method[^]
Cl			**671**	**32.26**	**3.76**	**12.54**[#]	
	Ni	red	670	32.20	3.81	12.43	
	Co	blue	671	32.48	3.83	12.55	
$HBpz_3$			**848**	**38.26**	**4.16**	**19.83**	
	Ni	purple	847	38.54	4.17	20.02	5
	Co	orange	848	38.50	4.18	20.18	5
$HBpz"_3$			**932**	**42.53**	**5.08**	**18.04**	
	Ni	purple	931	43.10	5.15	17.89	1
	Co	orange	932	42.54	5.20	18.04	4
$MeGapz_3$			**921**	**36.53**	**4.05**	**18.26**	
	Ni	blue	920	36.94	4.07	18.50	1
	Co	orange	921	36.39	4.16	18.05	2
$MeGapz"_3$			**1005**	**40.64**	**4.91**	**16.73**	
	Ni	green	1004	41.00	5.09	16.61	5
$\cdot 1.0\ CH_2Cl_2$				**38.56**	**4.71**	**15.42**	
	Co	orange	1005	38.36	4.67	15.24	5

Numbers in bold type are expected values. Cobalt and nickel atomic weights differ by only 0.22 g/mole therefore their expected microanalyses are very nearly identical.

$ Expected mass was calculated from average molecular weights (natural isotope abundance). The one mass unit difference observed in the spectra is due to the most abundant nickel isotope at mass 58 (68%) cf. cobalt at mass 59 (100 %).

^ Refer to pages 20-21.

Table 2.1.b Analytical Data of $HBpz^*_3ML$
(L = bis-chelating ligands)

L	Metal	Color	Mass$ (amu)	Microanalyses C	H	N	Purification Method
H_2Bpz_2			**782**	**36.88**	**4.26**	**17.92#**	
	Ni	blue	780	36.83	4.25	17.70	5
	Co	purple	781	37.18	4.22	17.75	5
Me_2Bpz_2			**810**	**38.57**	**4.61**	**17.30**	
	Ni	red	794	38.89	4.57	16.98	1
$\cdot 0.5\ CH_2Cl_2$				**37.20**	**4.49**	**16.41**	
	Co	purple	795	37.37	4.37	15.62	
Me_2Gapz_2			**869**	**35.95**	**4.29**	**16.13**	
	Ni	blue	853	36.01	4.20	16.16	3
	Co	red	854	36.28	4.20	15.45	5
$Me_2Gapz"_2 \cdot 0.5\ CH_2Cl_2$			**925**	**37.87**	**4.79**	**14.48**	
	Ni	green	909	38.16	4.83	14.20	3
	Co	purple	910	37.60	4.69	14.88	5
$Me_2Gapz(EA)$			**862**	**34.84**	**4.68**	**14.63**	
	Ni	blue		34.60	4.26	14.10	3
	Co	red		34.96	4.28	14.10	3
$Me_2Gapz"(EA)$			**890**	**36.44**	**4.98**	**14.17**	
	Ni	green	874	34.88	4.99	13.61	
	Co	purple	875	36.61	4.98	13.93	3

Numbers in bold type are expected values. Cobalt and nickel atomic weights differ by only 0.22 g/mole therefore their expected microanalyses are very nearly identical.

$ Expected mass was calculated from average molecular weights (natural isotope abundance). The one mass unit difference observed in the spectra is due to the most abundant nickel isotope at mass 58 (68%) cf. cobalt at mass 59 (100 %).

2.3 Characterization of Mixed Ligand Complexes

2.3.1 Mass Spectrometry

Mass spectrometry was used to confirm the molecular weight of each compound. All samples were analytically pure and were ionized by electron impact. In most cases parent peaks $[P]^+$ were observed. Complexes with terminal methyl groups on the boron or gallium atom easily lost a methyl group and peaks at $[P-15]^+$ were observed.

Isotopic patterns were used to identify a large number of fragments. The numbers reported always refer to the most intense mass to charge ratio (m/e) peak in any given isotopic pattern. This peak results from the most probable combination of isotopes in that particular fragment. These fragments contained at least one of boron, gallium, bromine or chlorine, all of which have natural isotopes. The isotopic patterns of these atoms and several combinations of them are shown in appendix 2.

The spectra of the cobalt complexes were selected as examples because cobalt has only one natural isotope [58 (100%)] where nickel has five [58 (67.9%), 60 (26.2%), 61 (1.2%), 62 (3.7%) and 64 (1.1%)]. The isotopic patterns of the cobalt complexes were less complicated and therefore easier to reconcile.

The mass spectrum of $HBpz^*_3CoCl$ is given as an example in Figure 2.5.

2.3.1a Mass Spectrum of $HBpz^*_3CoCl$

The $HBpz^*_3CoCl$ parent peak was seen at mass/charge (m/e) 671 (Fig. 2.5). Loss of HCl gave the most intense peak at m/e 633. There was an interesting recombination corresponding to the exchange of a bromide ligand with a chloride ligand on the parent molecule that gave the ion $[HBpz^*_3CoBr]^+$ at m/e 715.

Loss of Hpz^* from the de-chlorinated parent molecule gave $[Bpz^*_2Co]^+$ at m/e 445. This peak and the peak at m/e 633 were seen in the spectra of most of the mixed-ligand metal complexes. It seemed likely another pz^* moiety would have stripped off but this was not observed. Doubly charged species of the m/e 633 and 446 fragments were seen at m/e 317 and 223 , respectively.

Single isopropyl groups and single bromides were removed from $[Bpz^*_3Co]^+$ giving fragments at m/e 592 and 553, and $[Bpz^*_2Co]^+$ giving fragments at m/e 404 and 366.

Other important fragments were the $[Hpz^*B]^+$ at m/e 199, $[Hpz^*]^+$ at m/e 188, $[Hpz^*-Me]^+$ at m/e 173, $[pz]^+$ at m/e 66 and $[i-Pr]^+$ at m/e 43.

Some fragments under m/e 200 were due to ring opening of $[pz^*B]^+$. There are extensive rearrangement possibilities of borate and gallate complexes[20] which accounted for the large number of peaks in this region. Assignments of the other peaks are shown in table 2.2.

Figure 2.5 Mass Spectrum of $HBpz^*_3CoCl$

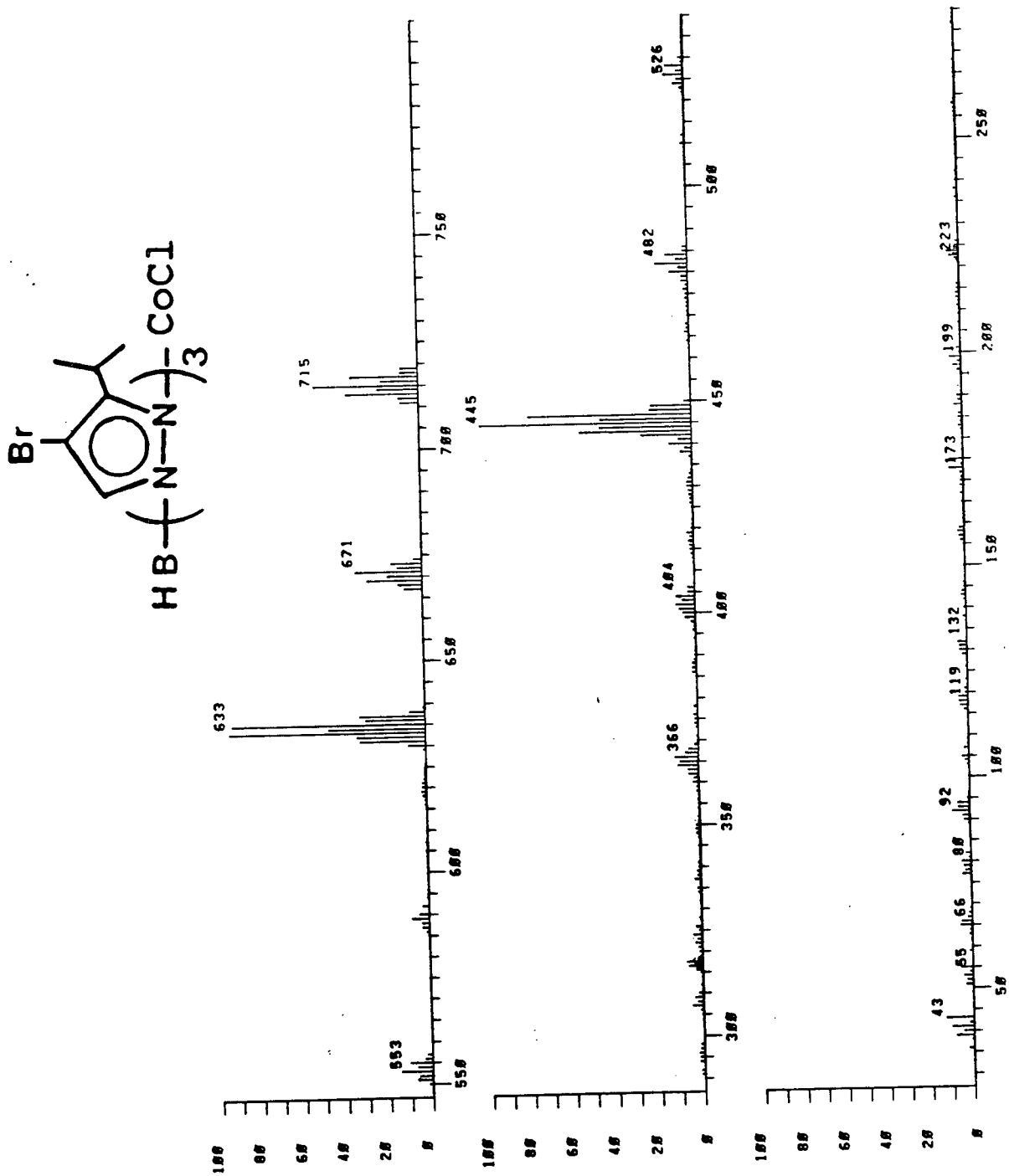

Table 2.2 Mass Spectral Assignments of $HBpz^*_3CoCl$

m/e	Intensity	Assignment
715	50	$[HBpz^*_3CoBr]^+$
671	35	$[HBpz^*_3CoCl]^+$
633	100	$[Bpz^*_3Co]^+$
592	<5	$[HBpz^*_2Co(4\text{-}Br\text{-}pz)]^+$
589	10	$[HBpz^*_2Co(3\text{-}iPr\text{-}pz)Cl]^+$
553	15	$[Bpz^*_2Co(3\text{-}iPr\text{-}pz)]^+$
526	15	$[Bpz^*_2CoBr]^+$
482	20	$[Bpz^*_2CoCl]^+$
445	100	$[Bpz^*_2Co]^+$
404	15	$[HBpz^*Co(4\text{-}Br\text{-}pz)]^+$
366	15	$[HBpz^*Co(3\text{-}iPr\text{-}pz)]^+$
317	10	m = 633; e = 2
223	10	m = 446; e = 2
199	10	$[Hpz^*B]^+$
188	10	$[Hpz^*]^+$
173	5	$[Hpz^* - Me]^+$
158	<5	$[Hpz^* - Me_2]^+$
132	5	$[BrCCCHN]^+$
119	5	$[(3\text{-}iPrpz)B]^+$
92	10	$[pzCCH_3]^+$
80	5	$[pzCH_3]^+$
66	5	$[Hpz]^+$
55	5	$[iPrC]^+$
43	15	$[iPr]^+$

2.3.1b Mass Spectrum of $HBpz^*_3Copz_3BH$

The mass spectrum of $HBpz^*_3Copz_3BH$ showed a low intensity parent peak at m/e 848. The peaks at m/e 633 and 445 corresponding to the $[HBpz^*_3Co]^+$ and $[HBpz^*_2Co]^+$ fragments (as seen in the previous spectrum) were not seen at all. Low intensity peaks were seen for fragments corresponding to the loss of pz and pz* from the parent at m/e 780 and 659 respectively. A fragment corresponding to the loss of both pz and pz* from the parent molecule was seen at m/e 580.

The major peak observed was the $[Bpz_3Co]^+$ fragment at m/e 271. This indicated that the $[HBpz_3]^-$ ligand formed the sturdier bond to the cobalt centre than did the $[HBpz^*_3]^-$ ligand. Loss of pz from $[Bpz_3Co]^+$ gave the $[Bpz_2Co]^+$ fragment at m/e 203. There were recombinations of $[Bpz_3Co]$ and $[Bpz_2Co]$ with the ligand fragments $[HBpz_3]$ and $[Bpz_2]$. The ions produced were of relatively high intensity corresponding to $[HBpz_3Copz_3B]^+$ at m/e 484, $[HBpz_3Copz_2B]^+$ at m/e 417 and $[(Bpz_2)_2Co]^+$ at m/e 348. This same phenomenon was observed in the mass spectra of the $HBpz^*_3Copz"_3BH$ and $HBpz^*_3Copz_3GaMe$ complexes. All of the other complexes listed in tables 2.1.a and 2.1.b displayed mass spectra more similar to that of the starting compound, $HBpz^*_3CoCl$, suggesting the $HBpz^*_3$ ligand formed the sturdier bond to the cobalt centre in those complexes.

Table 2.3 Mass Spectral Assignments of $HBpz^*_3Copz_3BH$

m/e	Intensity	Assignment
848	<5	$[HBpz^*_3Copz_3BH]^+$
780	<5	$[HBpz^*_3Copz_2B]^+$
659	<5	$[Bpz^*_2Copz_3BH]^+$
580	<5	$[Bpz^*_2Copz_2]^+$
484	70	$[HBpz_3Copz_3B]^+$
417	65	$[HBpz_3Copz_2B]^+$
348	25	$[(Bpz_2)_2Co]^+$
271	100	$[Bpz_3Co]^+$
262	30	$[MeCopz^*H]^+$
203	80	$[Bpz_2Co]^+$
188	25	$[pz^*]^+$
173	85	$[pz^*-Me]^+$
94	95	m = 188, e = 2
78	30	$[HpzC]^+$
68	45	$[Hpz]^+$
43	45	$[iPr]^+$
41	45	$[NNCH]^+$

2.3.1c Mass Spectrum of $HBpz^*_3Copz_2GaMe_2$

The parent peak of $HBpz^*_3Copz_2GaMe_2$ was seen as a trace in the spectrum at m/e 869. The major peak was observed at m/e 854 corresponding to the loss of a methyl group from the parent molecule. This was observed in all of the complexes incorporating the dimethyl bis-chelating ligands. The mass spectrum of $HBpz^*_3Copz_2GaMe_2$ has a similar fragmention pattern as that seen in mass spectrum of the starting compound, $HBpz^*_3CoCl$. In particular the peaks at m/e 633 and 445 corresponding to the fragments $[Bpz^*_3Co]^+$ and $[Copz^*_2BH]^+$ respectively were of high intensity in both spectra. These peaks were absent in the mass spectrum of $HBpz^*_3Copz_3BH$.

The introduction of gallium into the complexes produced new isotopic patterns that helped to identify the fragments. The fragment assignments are made in table 2.4.

Of particular interest were the recombinations at high molecular weights. The complex at m/e 854, corresponding to the fragment, $[HBpz^*_3Copz_2GaMe]^+$ picked up a pz moiety that gave the tris-chelated $[HBpz^*_3Copz_3GaMe]^+$ ion at m/e 921.

Another recombination was seen at m/e 974 which was attributed to the replacement of pz by pz* in the fragment, $[HBpz^*_3Copz_2GaMe]^+$ to give the ion $[HBpz^*_3Copz(pz^*)GaMe]^+$.

There appears to be dimerization of some of the small molecular weight gallium fragments. For example the peak at m/e 251 is consistent with $[Me_2GapzGaMe]^+$.

Table 2.4 Mass Spectral Assignments of $HBpz^*_3Copz_2GaMe_2$

m/e	Intensity	Assignment
974	20	$[HBpz^*_3Copz_2pz^*GaMe_2]^+$
921	5	$[HBpz^*_3Copz_3GaMe]^+$
869	<5	$[HBpz^*_3Copz_2GaMe_2]^+$
854	45	$[HBpz^*_3Copz_2GaMe]^+$
786	25	$[Bpz^*_3CopzGaMe]^+$
715	5	$[Bpz^*_3Copz_2Me]^+$
680	15	$[Bpz^*_2Copz_2GaMe_2]^+$
664	100	$[Bpz^*_2Copz_2GaMe]^+$
633	25	$[Bpz^*_3Co]^+$
620	5	$[Bpz^*(4\text{-}Br\text{-}pz)Copz_2GaMe]^+$
586	20	$[pz^*_2CopzGaMe]^+$
514	20	$[HBpz^*_2Copz]^+$
466	30	$[pz^*Copz_2GaMe]^+$
445	30	$[Copz^*_2BH]^+$
419	15	$[HBpz^*pz_2GaMe]^+$
392	20	$[pz^*pz_2Ga]^+$
358	20	$[BrCopz_2GaMe]^+$
332	25	m = 664 e = 2
251	10	$[MeGapzGaMe_2]^+$
205	10	$[Gapz_2]^+$
190	5	$[Hpz^*B]^+$
188	5	$[Hpz^*]^+$

continued

Table 2.4 continued

173	10	$[Hpz^*-Me]^+$
151	10	$[MeGapz]^+$
99	15	$[GaMe_2]^+$
94	10	m = 188 e = 2
79/81	<5	$[Br]^+$
78	5	$[Bpz]^+$
69/71	15	$[Ga]^+$
68	20	$[Hpz]^+$
55	10	$[iPrC]^+$
43	10	$[iPr]^+$
41	15	$[NNCH]^+$

2.3.2 X-ray Crystallography

Several crystal growth techniques were attempted as described in the experimental section of this chapter. The four coordinate starting compounds were recrystallized from benzene. A suitable single crystal of $HBpz^*_3CoCl$ was grown and the X-ray crystal structure was determined. The five coordinate complexes initially gave a viscous material that could be dried by heating to 70 ^oC under vacuum. These dried compounds were not hygroscopic but would rapidly pick up organic solvents from the glove box atmosphere to become viscous again. Several of the six coordinate complexes

effloresced once the solvent had been removed. Presumably the solvent was intrinsic to the crystal lattice but was weakly bound. A suitable single crystal of $HBpz^*_3Nipz"_3BH$ was grown from CH_2Cl_2 in the crystal growing apparatus and the X-ray crystal structure was determined.

2.3.2a The Solid State Molecular Structure of $HBpz^*_3CoCl$

The cobalt[II] centre in $HBpz^*_3CoCl$ (Fig. 2.6) is coordinated by three pyrazolyl nitrogens from the tris-chelating ligand and one chloride ligand. The mean Co-N bond length is 2.045(7) A and the average N-Co-N bond angle is 94.4(3)°. Comparing these data with the Co-Cl bond distance of 2.207(3) A and average N-Co-Cl bond angle of 122.1(3)°, it is clear that the three nitrogens form the base of a trigonal pyramidal structure with the chloride at the apex.

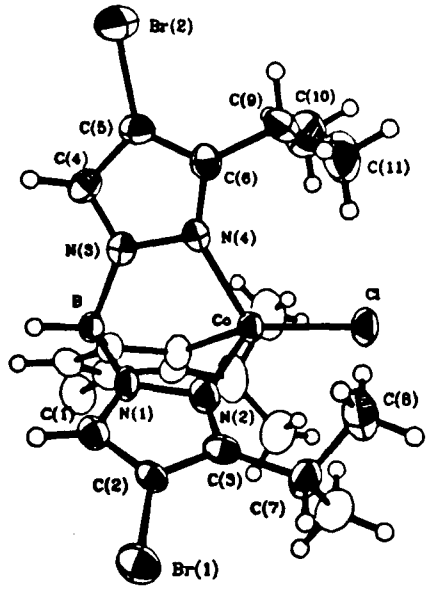

Figure 2.6 Solid State Molecular Structure of $HBpz^*_3CoCl$

This structure then has C_{3v} symmetry with the 3-fold axis along the Co-Cl bond. The isopropyl groups at the 3 position are arranged such that the two methyl groups are bent toward the metal centre.

A stereoscopic view of the structure, crystallographic parameters and bond lengths and angles are in appendix 3.a.

2.3.2b The Solid State Molecular Structure of $HBpz^*_3Nipz"_3BH$

The nickel[II] centre of $HBpz^*_3Nipz"_3BH$ (Fig. 2.7) is coordinated by six pyrazolyl nitrogens. The three nitrogens coordinating the nickel from the $HBpz"_3$ ligand have mean Ni-N bond lengths of 2.07(1) A and average N-Ni-N bond angles of 88.9(5)°. The three coordinating nitrogens from the $HBpz^*_3$ ligand have mean N-Ni bond lengths of 2.15(1) A and average N-Ni-N bond angles of 89.0(5)°.

In the structure the trans-nitrogens are at a mean angle of 179.4(5)° and so the six nitrogen metal bonds lie on Cartesian axes with nickel at the origin. The molecule has C_{3v} symmetry along the B-Ni-B axis.

A conformational change has been brought about by the coordination of the tris(3,5-dimethylpyrazolyl)borate ligand. The isopropyl methyl groups are now pointing away from the metal centre (cf $HBpz^*_3CoCl$).

A stereoscopic view of the structure, crystallographic parameters and bond lengths and angles are listed in appendix 3.b.

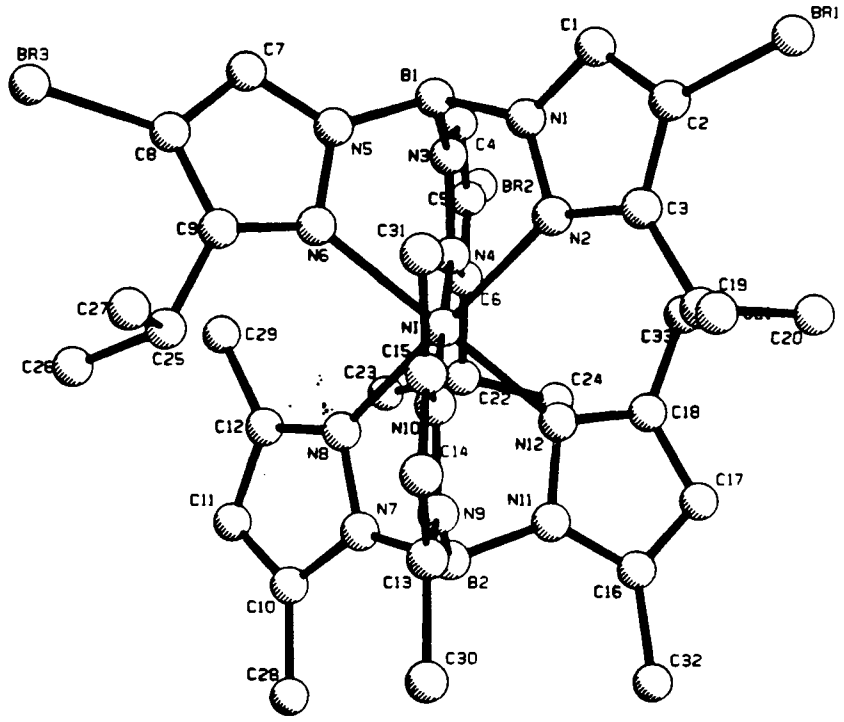

Figure 2.7 Solid State Molecular Structure of $HBpz^{*}_{3}Nipz"_{3}BH$

2.3.3 Electronic Spectroscopy

The electronic transitions of the solvated, mixed-ligand complexes were investigated by recording absorption spectra from the near infrared to the ultra-violet region (4,000 cm^{-1} to 40,000 cm^{-1}). The series included four, five and six coordinate complexes (Tables 2.5.a and 2.5.b, page 36). All spectra were done with analytically pure samples dissolved in benzene, against a benzene reference.

Table 2.5.a UV/Vis Spectroscopic Data of $HBpz^*_3NiL$ &
(L = mono- and tris-chelating ligands)

L	Dq (cm^{-1})	B (cm^{-1})@	Absorption Peaks (cm^{-1})# *Extinction Coefficients* ($Lmol^{-1}cm^{-1}$)					
Cl	680	1030	36000	20800	17900	12400	10900	6060
			970	*500*	*100*	*92*	*440*	*130*
$HBpz_3$	1140	823	36000	28900	18100	11400		
			100	*17*	*7*	*4*		
$HBpz"_3$	1090	720	36000	26500	17400	10900		
			330	*28*	*8*	*8*		
$MeGapz_3$	1080	740	36000	26800	17200	10800		
			80	*11*	*5*	*6*		
$MeGapz"_3$	924	740	36000	24300	14900			
			1800	*30*	*10*			

Table 2.5.b UV/Vis Spectroscopic Data of $HBpz^*_3NiL$ &
(L = bis chelate ligands)

L	Absorption Peaks (cm^{-1})# *Extinction Coefficients* ($Lmol^{-1}cm^{-1}$)					
H_2Bpz_2	36000	32900	26700	17400	11700	6900
	700	*230*	*100*	*22*	*28*	*170*
Me_2Bpz_2	36000	32300	27000	18200	11500	6540
	550	*200*	*220*	*140*	*1*	*9*
Me_2Gapz_2	36000	32700	26500	16800	11400	6710
	600	*220*	*100*	*17*	*30*	*272*
$Me_2Gapz"_2$	36000	31700	25700	15900	11200	6620
	440	*293*	*80*	*11*	*70*	*460*

& Dissolved in benzene.
# Errors in absorption peak positions were determined by successive measurements and were of the order of 1-2%.
@ Nickel free ion Racah parameter B^o = 1080 cm^{-1}

One method of interpreting electronic spectra is to assume a higher symmetry of the complex than is actually present. The electronic spectra of nickel[II] complexes in particular have been well interpreted in this way [21,22,23]. The method assumes that the ligands are equivalent point dipoles and are arranged in the highest realistic symmetry. For example the six coordinate complexes can be assumed to be of octahedral (O_h) symmetry. This method is only an approximation and deviations from the higher symmetries will cause splitting of degenerate electronic levels. Broad bands are expected and observed in these spectra.

In a series of compounds with similar symmetries and coordination numbers it would be expected that shifts in the absorption peaks reflect the ligand field strengths. Both the crystal field splitting energy (10 D_q) and the Racah parameter (B) are calculated for each complex and comparisons of the ligand field strengths are made.

Electronic transitions are not allowed between states of like parities (Laporte forbidden). These parities are symmetry elements that arise from a centre of inversion and are either odd (*u*) or even (*g*). The d orbitals have g symmetry so d -> d transitions (*g* -> *g*) are forbidden and small extinction coefficients are expected. Octahedral complexes have ligands arranged such that the transition metal is a centre of inversion. The octahedral ligand field then does not disturb the parity of the d orbitals. However the tetrahedral ligand field does not have an inversion

centre and distorts the *g* symmetry of the d orbitals. The result is that the forbiddeness of d -> d transitions in tetrahedral complexes is relaxed. Higher extinction coefficients are expected in the electronic transitions of tetrahedral complexes than of octahedral complexes. A comparison of the extinction coefficients in Tables 2.5.a and 2.5.b shows this trend. The macroscopic effect of this is seen in the darker colors of the four coordinate complexes compared with the paler colors of the six coordinate complexes.

2.3.3a The Tetrahedal Approximation of $HBpz^*_3NiCl$

A tetrahedral ligand field model is used to predict the allowed electronic transition energies of $HBpz^*_3NiCl$.

The transitions for a d^8, tetrahedral complex are:

$^3T_1$	----->	$^3T_2$	ν_1
	----->	$^3A_2$	ν_2
	----->	$^3T_1(P)$	ν_3
	----->	$^1E(D)$	spin forbidden
	----->	$^1T_2(G)$	spin forbidden

There are three spin allowed and two spin forbidden transitions. The observed peaks are compared with a calculated fit from Tanabe-Sugano diagrams for a d^8 tetrahedral ligand environment (Fig. 2.9, Table 2.6).

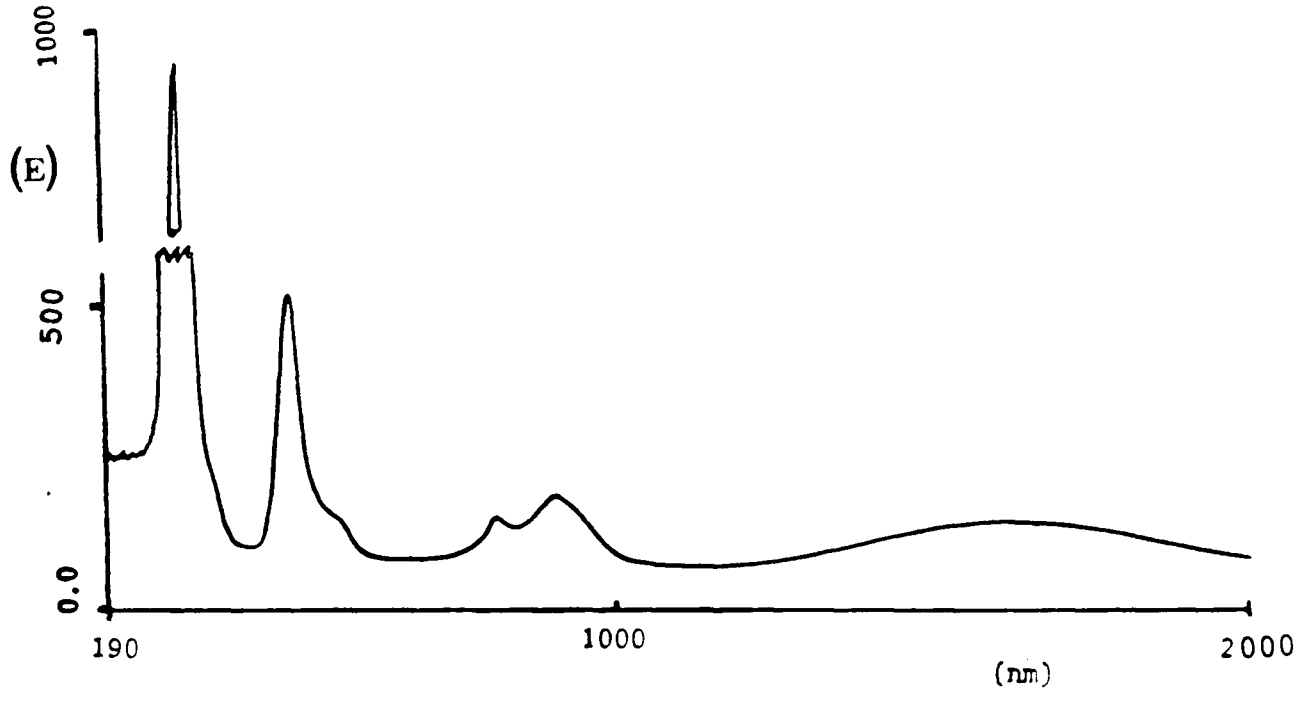

Figure 2.9 Electronic Spectrum of $HBpz^*_3NiCl$

Table 2.6 Calculated and Observed Electronic Transition Energies of $HBpz^*_3NiCl$

Observed (cm^{-1})	Calculated (cm^{-1})	Assignment
6060 (130)#	5790	ν_1
10900 (440)		$^1E(D)$
12400 (92)	12400	ν_2
17900 (100)		$^1T_2(G)$
20800 (500)	20300	ν_3
36000 (970)		C.T.@

@ Charge transfer band # Extinction coefficients

The D_q and B values calculated are : D_q = 680 cm^{-1}; B = 1030 cm^{-1}.

The calculated and observed spin allowed transitions energies fit within 3 %. The close fit supports the assignment of near tetrahedral symmetry to the four coordinate complex in solution.

The spin forbidden transitions from the triplet ground state to the singlet excited states are assigned to the bands at 17,900 cm^{-1} ($^3A_2 \rightarrow {}^1T_2$) and 10,870 cm^{-1} ($^3A_2 \rightarrow {}^1E$).

A descent of symmetry to a trigonal pyramidal (C_{3v}) geometry would cause splitting of the triplet terms and band broadening.

2.3.3b The Octahedral Approximation of $HBpz^*_3Nipz"_3BH$

The crystal structure of $HBpz^*_3Nipz"_3BH$ showed a very nearly octahedral structure so an octahedral ligand field model might be expected to be a good approximation.

The expected transitions for a d^8 octahedral are:

$^3A_{2g}$	----->	$^3T_{2g}$	ν_1
	----->	$^3T_{1g}$	ν_2
	----->	$^3T_{1g}(P)$	ν_3
	----->	$^1E_g(D)$	spin forbidden
	----->	$^1T_{2g}(D)$	spin forbidden

There are three spin allowed and two spin forbidden transitions. The observed peaks are compared with a

calculated fit from Tanabe-Sugano diagrams for a d^8 octahedral ligand environment (Fig. 2.10, Table 2.7).

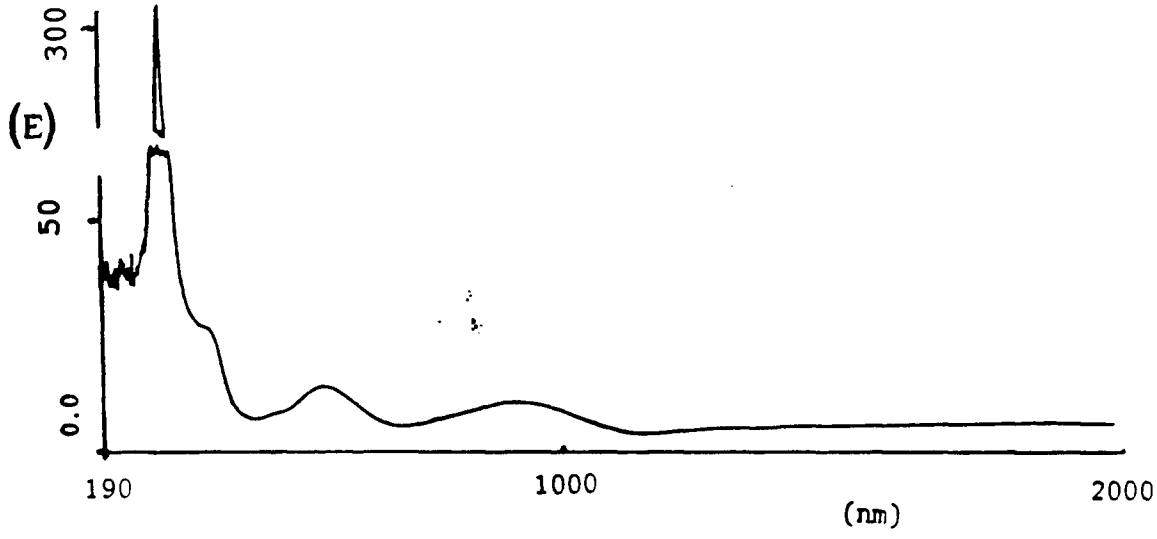

Figure 2.10 Electronic Spectrum of $HBpz^*_3Nipz"_3BH$

Table 2.7 Calculated and Observed Electronic Transition Energies of $HBpz^*_3Nipz"_3BH$

Observed (cm^{-1})		Calculated (cm^{-1})	Assignment
10900	(8)	10900	ν_1
17400	(8)	17000	ν_2
26500	(28)	26500	ν_3
36000	(330)		C.T.

The D_q and B values calculated are : D_q = 720 cm^{-1}; B = 1090 cm^{-1}.

The calculated and observed transition energies fit within 3 %. The close fit supports the assignment of near octahedral symmetry to the six coordinate complex in solution.

A descent of symmetry would cause a splitting of the triplet state terms and the broadening of bands.

A comparison of the crystal field splittings (10 D_q) of the nickel octahedral complexes (Table 2.5.a) showed that when complexed with $HBpz^*_3NiCl$ the ligands were ordered, from strong field ligand to weak field ligand as $HBpz_3$ > $HBpz"_3$ ~ $MeGapz_3$ > $MeGapz"_3$.

A stronger field ligand would be expected to be either a strong base that would bind tightly to the metal centre or sterically small so that it can physically approach the metal more closely. If electronic effects were dominant then the higher electronegativity of boron would make the pyrazolyl ring more acidic and so a weaker field ligand than the gallium analog. However, just the reverse is seen. Methyl substitutions at the 3 and 5 positions on the pyrazolyl ring would make the ring more basic (inductive effect) and so a stronger field ligand, but again the opposite is observed. The ligand field strength is not an electronic effect. Steric conditions imposed by the bulky ligand, $[HB(3\text{-}iPr\text{-}4\text{-}Br\text{-}pz)_3]^-$ around the metal centre has determined the ligand field strength of this series.

2.3.3c Five Coordinate Nickel[II] Complexes

There are crystal field models that have been proposed for high spin nickel[II] complexes in both trigonal bipyramidal (D_{3h}) and square pyramidal (C_{4v}) configurations[22]. An attempt was made to fit the electronic spectrum of $HBpz^*_3Nipz_2BH_2$ to these models (Table 2.8).

Table 2.8 Calculated and Observed Electronic Transition Energies of $HBpz^*_3Nipz_2BH_2$

Observed (cm^{-1})	Calculated (cm^{-1})	Calculated (cm^{-1})	Calculated (cm^{-1})
	D_{3h}	C_{4v}	O_h
6900 (170)	6900	6900	
11700 (28)	13500	9320	11700
17400 (22)	14600	14100	17500
26700 (100)	22500	23200	27200
32500 (230)	26400	39300	C.T.
36000 (700)	C.T.	C.T.	C.T.

It is clear that neither model fits the observed spectrum so $HBpz^*_3Nipz_2BH_2$ possess neither of these symmetries.

There are a few examples of five coordinate nickel[II] complexes whose electronic transition energies fit the trigonal bipyramidal model[24,25]. The crystal structure of

one such complex, $Me_2Gapz"(OCH_2CH_2NMe_2)Nipz"_2GaMe_2$, showed a distorted trigonal bipyramidal stucture. The crystal structure also showed the unsymmetrical tridentate pyrazolylgallate ligand, $[Me_2Gapz"(OCH_2CH_2NMe_2)]^-$ coordinated in a meridonal fashion, which may be instrumental in the stuctural symmetry. The $[HBpz^*_3]^-$ ligand used in the mixed-ligand complex series will only coordinate in a facial manner.

The UV/Vis spectra of the five coordinate complexes showed an additional band at 32,500 cm^{-1} (as a shoulder) that is not seen in the spectra of the four or six coordinate complexes (cf. Fig. 2.10 and Fig. 2.11). The extinction coefficient of this band is not large (200-410 $Lmol^{-1}cm^{-1}$) and initially it seemed the band could be

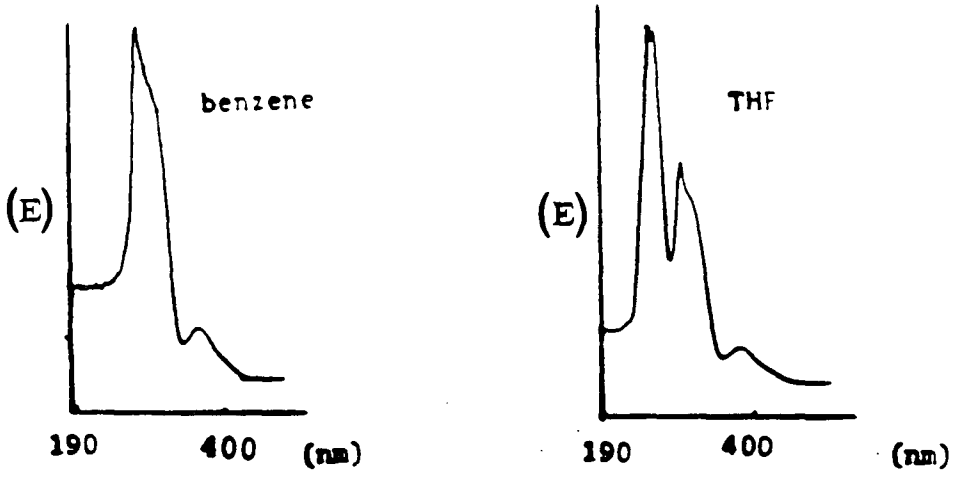

Figure 2.11 UV/Vis Spectra of $HBpz^*_3Nipz_2BH_2$ in Benzene and THF as Solvents

assigned as a charge transfer resulting from a coordinated benzene molecule. However a comparison of the electronic spectra of $HBpz^*_3Nipz_2BH_2$ recorded with different solvents

(benzene and THF) showed only a slight shift in bands. If a benzene molecule had been coordinated there should have been a loss of a charge transfer band. The appearance of a new band at 41,500 cm^{-1} (Fig. 2.11) suggested that a THF molecule had coordinated.

In anticipation of an octahedral complex a fit to an octahedral symmetry was calculated (Table 2.8) and the fit was reasonably good. The high band at 32,500 cm^{-1} could be assigned to a charge transfer but the low band at 6090 cm^{-1} could not be assigned therefore making the O_h model inappropriate.

2.4 Conclusion

The syntheses and purifications of the mixed ligand compounds were refined to give good yields (60-90%) of analytically pure products.

The mass spectral evidence showed that the $HBpz_3^-$, $HBpz"_3^-$ and $MeGapz_3^-$ ligands bound more tightly to the metal center than any of the other ligands in the series as evidenced by the appearance of intense peaks at masses corresponding to the ions $[HBpz_3M]^+$, $[HBpz"_3M]^+$ and $[MeGapz_3M]^+$, respectively (M = Ni,Co).

Numerous crystal growth techniques were attempted but crystals of only two compounds, $HBpz^*_3CoCl$ and $HBpz^*_3Nipz"_3BH$, suitable for X-ray crystallography were produced.

The crystal structure of the starting material, $HBpz^*_3CoCl$ determined that the solid state structure of the complex was four coordinate and of C_{3v} symmetry. The three pyrazolyl nitrogens coordinating the metal formed the base of a trigonal pyramidal structure with the chlorine ligand at the apex.

The crystal structure of $HBpz^*_3Nipz"_3BH$ showed that the solid state structure of the complex was six coordinate and very nearly octahedral in the arrangement of the two tris chelating ligands. The structure also showed a conformational change that was imparted to the $[HBpz^*_3Ni]^+$ complex on coordination of the $HBpz"_3^-$ ligand by rotation of the isopropyl group in the 3 position of the pz^* ring.

The electronic spectral evidenced showed the geometry of the four coordinate complex, $HBpz^*_3NiCl$ was approximated by atetrahedral symmetry.

Similarly the six coordinate complex geometry was approximated by an octahedral symmetry. A comparison of the crystal field splitting energies of the octahedral complexes gave a ligand field strength order of $HBpz_3$ > $HBpz"_3$ ~ $MeGapz_3$ > $MeGapz"_3$ when complexed with $HBpz^*_3NiCl$. This order was as a result of the steric control of the active pocket by the intermediate ligand $[HBpz^*_3]^-$.

The five coordinate complexes fit neither a trigonal bipyramidal (D_{3h}) nor square pyramidal (C_{4v}) model. The attempt to fit an octahedral symmetry was also unsuccessful because of an unassignable band at 6900 cm^{-1}. Further work

needs to be done to elucidate the structures of these complexes.

The active pocket created by Trofimenko's intermediate ligand in the complexes $[HBpz^*_3]MCl$ have been probed by the characterization of the series of mixed-ligand complexes. The series demonstrated preferential binding of some ligands, steric control of substrate ligands and conformational changes in the metal complexes on coordination of a substrate ligand.

Chapter III

Rhodium[I] Complexes of Unsymmetrical Pyrazolylgallate Ligands and Their Reactivity

3.1 Introduction

There are a number of four coordinate rhodium[I] complexes that have been reported to show catalytic activity. These complexes are sixteen electron species and are expected to readily undergo oxidative additions. This is an important step in catalytic activity. Oxidative addition to a rhodium[I] complex produces a six coordinate, rhodium[III] complex. The reverse reaction, reductive elimination of a rhodium[III] complex, must also take place to complete a catalytic cycle, regenerating a four coordinate rhodium[I] complex. A square planar, rhodium[I] complex is also coordinatively unsaturated, providing empty coordination sites for incoming substrates, another important feature of a catalytic reagent.

When looking for catalytic activity in a new species it is important to look at the intermediate steps in successfully catalysed reactions. Wilkinson's catalyst, $Rh(PPh_3)_3Cl$, is perhaps the most known for its catalytic hydrogenation of alkenes[26]. The catalytic steps include oxidative addition of H_2 and π bonding of an alkene. Another important rhodium[I] catalytic reagent is

$RhH(CO)(PPh_3)_2$, used in the hydroformylation of alkenes[27]. The catalytic steps include oxidative addition of H_2, π bonding of an alkene and addition and insertion of carbon monoxide. The Monsanto reagent, $Rh(CO)_2I_2$, is used as a catalyst in the synthesis of acetic acid[28]. Important steps in this reaction are the oxidative addition of CH_3I and addition and insertion of carbon monoxide. Another important reaction that has catalytic significance is the activation of carbon-hydrogen bonds (ie. oxidative addition of R-H). A number of five coordinate rhodium[I] complexes have been reported that show this type of activity[29,30].

Interest in the unsymmetric, tridentate pyrazolylgallate ligands in catalysis arose with reports that complexes of formula LRh(CO) (L = $Me_2Gapz(OCH_2CH_2NMe_2)$[31], $Me_2Gapz(OC_9H_6N)$[32], $Me_2Gapz(OCH_2(C_5H_4N)$[33]) have shown oxidative addition of MeI and the subsequent insertion of a carbonyl into the rhodium-methyl bond (Fig. 3.0).

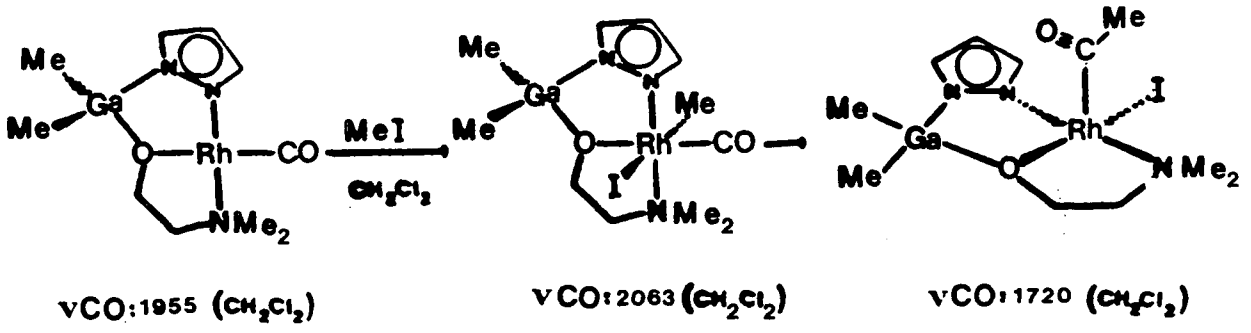

Figure 3.0 Oxidative Addition of MeI and Carbonyl Insertion on $Me_2Gapz(OCH_2CH_2NMe_2)Rh(CO)$

This activity prompted further investigations of similar rhodium[I] complexes and the results are reported in this chapter.

The unsymmetric, tridentate pyrazolylgallate ligands are derived from the $[Me_2Gapz_2]^-$ ligand by replacement of one of the pyrazolyl rings with a bifunctional moiety (Fig 3.1). Tris chelation can take place through the electron lone pairs on the nitrogen of the pyrazolyl ring and the donor atoms (X and Y) of the bifunctional moiety. The donor atoms may be varied and substituents may be added to the pyrazolyl ring providing steric and electronic control. The carbon fragment of the bifunctional moiety may be varied and through adroit substitutions can control the coordination mode of the ligand. These ligands have been shown to be able to coordinate to transition metals in either a facial or meridional fashion[24]. The coordination mode of the ligand may be important in binding a substrate to the metal centre.

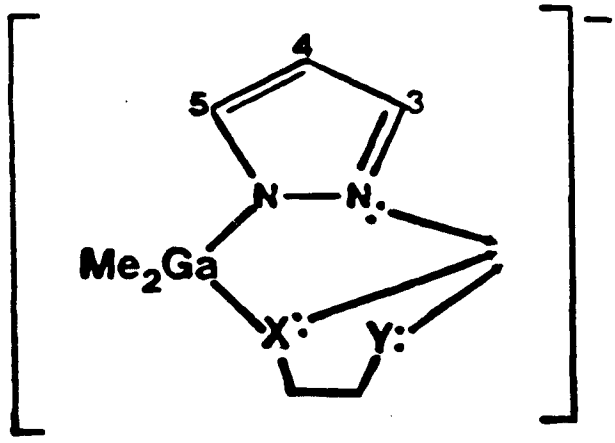

Figure 3.1 Tris-Chelating Unsymmetric Pyrazolylgallate Ligand

A common catalytic step is the loss of a ligand to free a coordination site for substrate binding. The subsequent reattachment of the ligand to complete the catalytic cycle suggested the use of a multidentate ligand. The reasoning is that if the displaced ligand were an arm on a multidentate ligand, it would be held nearby for a more expedient re-attachment. The unsymmetric pyrazolylgallates ligands seemed to offer this potential.

In this chapter the preparations and reactivities of two rhodium[I] complexes, incorporating the unsymmetric pyrazolylgallates ligands, are described. The two ligands used were prepared by varying only the Y group. The pyrazolyl ring was unsubstituted, the X donor was oxygen and the carbon chain was $-CH_2-CH_2-$. The Y donor groups were $-NH_2$ and $-CH=CH_2$ and were abbreviated (EA) for ethanolamino and (but) for but-3-enolate.

3.2 Experimental

The syntheses of $Na^+[Me_2Gapz(EA)]^-$ and $Na^+[Me_2Gapz(but)]^-$ are reported in chapter 2. All reactions were carried out under a nitrogen atmosphere. Solvents were purified by the methods described in chapter 2. Microanalyses were attempted on all compounds and those that gave satisfactory results are reported.

3.2.1 Preparation of $Me_2Gapz(EA)Rh(CO)$

$$Na^+[Me_2Gapz(EA)]^- + 1/2[Rh(CO)_2Cl]_2 \xrightarrow[\text{reflux}]{------>} Me_2Gapz(EA)Rh(CO) + CO + NaCl$$

Two molar equivalents of $Na^+[Me_2Gapz(EA)]^-$ (1.02 mmole) in THF were added to a molar equivalent of rhodium dimer (0.198 g; 0.510 mmole) dissolved in 150 ml of THF. The mixture was refluxed under a nitrogen atmosphere for 16 hours. The disappearance of the rhodium dimer carbonyl stretches at 2070 and 1985 cm^{-1} (THF) in the IR spectrum and the appearance of the product monocarbonyl stretch at 1945 cm^{-1} (THF) monitored the progress of the reaction (Fig. 3.2). The mixture was made up to a known volume with THF and stored under nitrogen.

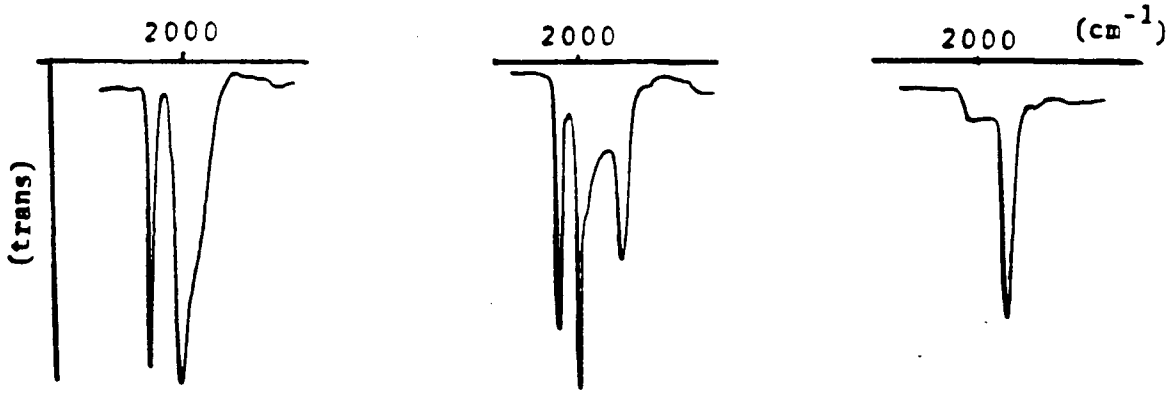

$[Rh(CO)_2Cl]_2$ 3 hour reflux $Me_2Gapz(EA)Rh(CO)$

Figure 3.2 IR Spectra of $[Rh(CO)_2Cl]_2$, the reaction mixture after a 3 hour reflux and $Me_2Gapz(EA)Rh(CO)$

3.2.2 Preparation of $Me_2Gapz(but)Rh(CO)$

$$Na^+[Me_2Gapz(but)]^- + 1/2\ [Rh(CO)_2Cl]_2 \xrightarrow[\text{reflux}]{------} Me_2Gapz(but)Rh(CO) + CO + NaCl$$

Two molar equivalents of $Na^+[Me_2Gapz(but)]^-$ (2.77 mmole) in THF were added to a molar equivalent of rhodium dimer (0.538 g; 1.38 mmole) dissolved in 150 ml of THF. The mixture was refluxed under a nitrogen atmosphere for 18 hours. The disappearance of the rhodium dimer carbonyl stretches at 2070 and 1985 cm^{-1} (THF) in the IR spectrum and the appearance of the monocarbonyl stretch at 1995 cm^{-1} (THF) monitored the progress of the reaction. The mixture was made up to a known volume with THF and stored under a nitrogen atmosphere.

3.2.3 Attempted Preparation of $Me_2Gapz"(EA)Rh(CO)$

$$Na^+[Me_2Gapz"(EA)]^- + 1/2\ [Rh(CO)_2Cl]_2 \xrightarrow[\text{reflux}]{--\not{x}-->} Me_2Gapz"(EA)Rh(CO) + CO + NaCl$$

The reaction was carried out in a similar fashion as the above reactions. The reaction mixture was refluxed for 18 hours under a nitrogen atmosphere. The rhodium dimer carbonyl stretches in the IR spectrum at 2070 and 1985 cm^{-1} (THF) were replaced by carbonyl stretches at 2098, 2075 and 2020 cm^{-1} (THF). The solvent was stripped off under vacuum

leaving a brown solid. This solid was redissolved in CH_2Cl_2 and the mixture was filtered. The solvent was allowed to evaporate slowly to promote crystal growth. The isolated compound analysed for $C_7H_7N_2O_2Rh$, as the probable dimer $[Rh(CO)_2pz"]_2$.

Microanalysis: $[Rh(CO)_2pz"]_2$

Calc.	C	33.08	H	2.76	N	11.03
Found	C	33.31	H	3.02	N	10.80

3.2.4 Reactions of Rh[I] Complexes

Oxidative addition, addition and carbon-hydrogen bond activation reactions were attempted with both $Me_2Gapz(EA)Rh(CO)$ and $Me_2Gapz(but)Rh(CO)$.

Reactions were monitored by changes in the IR spectrum of the carbonyl region. The ability of the rhodium centre to back bond to the carbonyl antibonding orbitals will be affected by the oxidation state of the metal and the electron donating ability of the ligands. The more electron density about the metal center, the weaker the carbonyl stretch.

3.2.4a Oxidative Addition Reactions

An excess of MeI was added to a stirred THF solution of $Me_2Gapz(EA)Rh(CO)$ and the mixture was refluxed for one hour.

The carbonyl stretching frequencies in the IR spectrum shifted from 1945 cm^{-1} (THF) to 2030 cm^{-1} (THF). The higher C-O stretch of the product was consistent with a higher oxidation state of the rhodium centre. Oxidative addition of MeI to the rhodium[I] complex would produce the six coordinate rhodium[III] adduct, Me_2Gapz(EA)Rh(CO)(Me)I (Fig 3.3.a). The solvent was removed under vacuum leaving a dark red solid. This solid was redissolved in CH_2Cl_2 and the mixture was filtered. The solvent was allowed to evaporate slowly to promote crystal growth. The isolated compound was unidentifiable by microanalysis.

A carbonyl insertion into the newly formed rhodium-methyl bond was anticipated but there was no evidence of an acetyl group in the IR spectrum of the product.

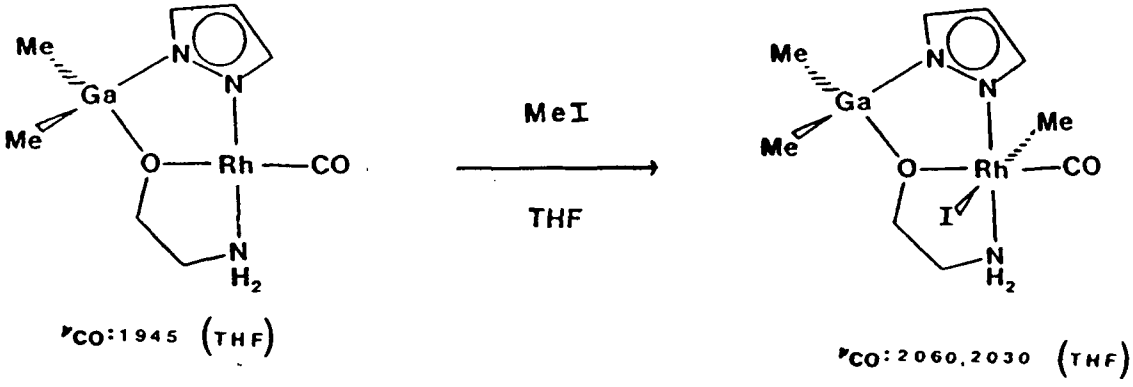

Figure 3.3.a Preparation of Me_2Gapz(EA)Rh(CO)(Me)(I)

In a subsequent reaction the mixture was refluxed for 4 days. The carbonyl stretch shifted from 2030 cm^{-1} (THF) to 2060 cm^{-1} (THF). The solvent was removed under vacuum leaving a dark red solid. This solid was redissolved in

CH_2Cl_2 and the mixture filtered. The slow evaporation of solvent left a solid that analysed as $C_9H_{18}N_3O_2I_2Rh$.

Microanalysis: $Me_2Gapz(EA)Rh(CO)(Me)I_2$

Calc.	C	17.24	H	2.89	N	6.71
Found	C	17.62	H	2.97	N	6.81

This compound was the net addition of MeI_2 to $Me_2Gapz(EA)Rh(CO)$ to give $Me_2Gapz(EA)Rh(CO)(Me)I_2$. The way in which the MeI_2 was incorporated into the structure is not clear. It is unlikely the second iodide was bonded to the rhodium centre because that would have produced a rhodium[IV] complex. The complex may have been an iodo salt of a rhodium[III] cationic complex which a conductivity measure would have established as a possibility.

An excess of I_2 was added to a THF solution of $Me_2Gapz(EA)Rh(CO)$ and the mixture refluxed for 2 hours. The carbonyl stretch in the IR spectrum shifted from 1945 cm^{-1} (THF) to 2095 cm^{-1} (THF). The shift was consistent with an oxidative addition of I_2 to produce the complex $Me_2Gapz(EA)Rh(CO)I_2$ (Fig. 3.3.b). The solvent was removed under vacuum leaving a reddish-brown solid. This solid was redissolved in CH_2Cl_2 and the mixture filtered. The solvent was allowed to evaporate slowly. The isolated solid was unidentifiable.

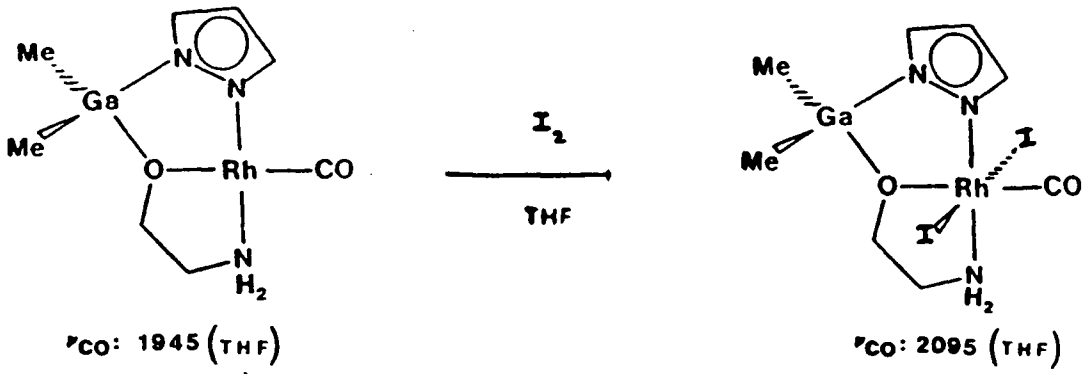

Figure 3.3.b Preparation of $Me_2Gapz(EA)Rh(CO)I_2$

An excess of allyl bromide was added to a solution of $Me_2Gapz(EA)Rh(CO)$ in THF and stirred for one hour. The carbonyl stretch in the IR spectrum shifted from 1945 cm^{-1} (THF) to 2065 cm^{-1} (THF) which was consistent with an oxidative addition of allyl bromide (Fig. 3.3.c) to produce the complex, $Me_2Gapz(EA)Rh(CO)(allyl)Br$. When the reaction mixture was refluxed for one hour, the carbonyl band in the IR spectrum disappeared. Presumably the ~~π~~ allyl complex,

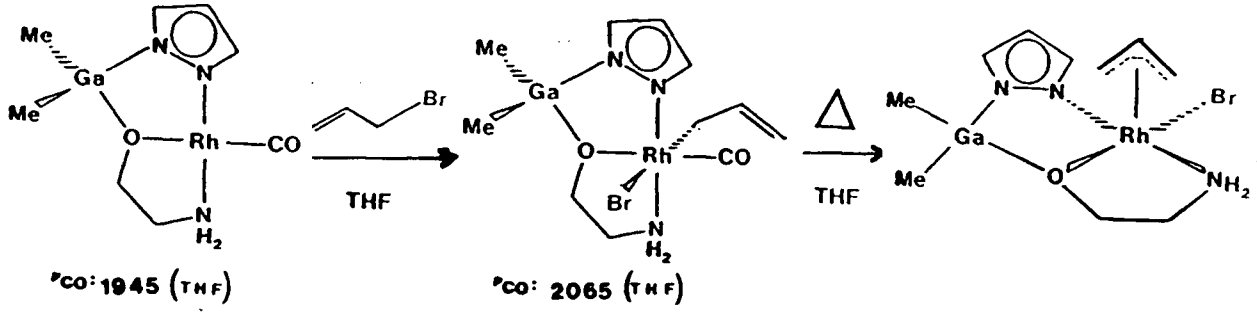

Figures 3.3.c $Me_2Gapz(EA)Rh(CO)(allyl)Br$
3.3.d $Me_2Gapz(EA)Rh(n^3\text{-allyl})Br$

$Me_2Gapz(EA)Rh(n^3\text{-allyl})Br$ was produced through loss of a carbonyl ligand (Fig. 3.3.d). Neither product was successfully isolated.

3.2.4b Addition Reactions

Carbon monoxide was bubbled through a cold (0°C) THF solution of $Me_2Gapz(EA)Rh(CO)$ for one hour. The 1945 cm^{-1} carbonyl stretch was replaced by bands at 2075 and 2015 cm^{-1} which is consistent with the dicarbonyl species, $Me_2Gapz(EA)Rh(CO)_2$ (Fig. 3.3.e). The compound was not successfully isolated.

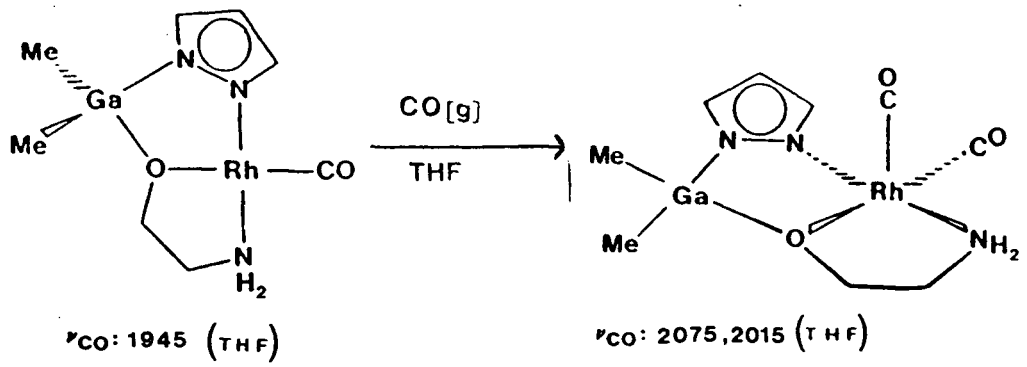

Figures 3.3.e $Me_2Gapz(EA)Rh(CO)_2$

Ethene was bubbled through a cold (0°C) THF solution of $Me_2Gapz(EA)Rh(CO)$ for one hour. The 1945 cm^{-1} carbonyl stretch was replaced by two bands at 2075 and 2005 cm^{-1} suggesting the formation of isomers of the ethene adduct (Fig. 3.3.f). This compound was recrystallized from

methylene chloride and analysed as $Me_2Gapz(EA)Rh(CO)(ethene) \cdot 0.5\ CH_2Cl_2$.

Microanalysis: $Me_2Gapz(EA)Rh(CO)(ethene) \cdot 0.5\ CH_2Cl_2$

Calc.	C	29.30	H	4.70	N	9.79
Found	C	29.01	H	4.61	N	9.70

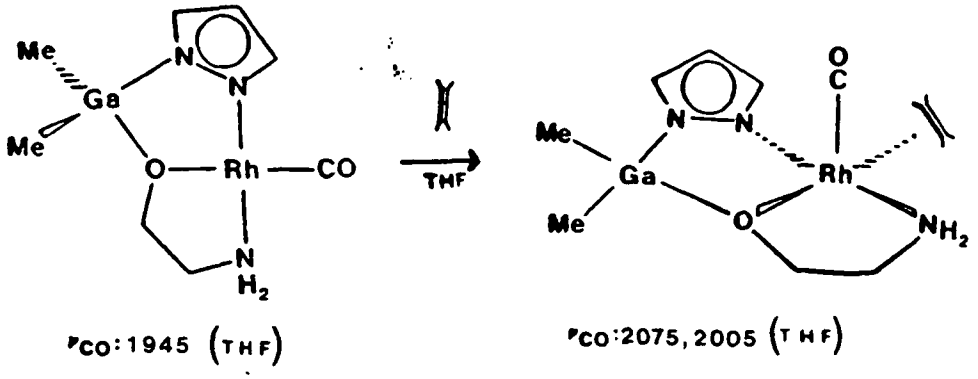

Figures 3.3.f $Me_2Gapz(EA)Rh(CO)(ethene)$

3.2.4c Activation of Carbon-Hydrogen Bonds

There are a few tripodal ligand systems reported that activate carbon-hydrogen bonds[29,30]. The pyrazolyl based complex, $HBpz"_3Rh(CO)_2$, reported by Graham et al., photochemically activates aromatic and saturated hydrocarbons. For example, when a benzene solution of $HBpz"_3Rh(CO)_2$ is irradiated for 5 minutes with a mercury lamp there is complete conversion to $HBpz"_3Rh(CO)(C_6H_5)(H)$.

The success of $HBpz"_3Rh(CO)_2$ as a carbon-hydrogen bond activator prompted the investigation of the unsymmetrical

tridentate pyrazolylgallate rhodium[I] carbonyl complexes, $LRh(CO)$ (L = $Me_2Gapz(OCH_2CH_2NH_2)$, $Me_2Gapz(OCH_2CH_2CH=CH_2)$) for this type of behaviour. Additionally, both of these complexes readily added a carbonyl forming the five coordinate, dicarbonyl adduct, $LRh(CO)_2$, that was analogous to the $HBpz"_3Rh(CO)_2$ complex reported by Graham.

An attempt was made to activate the carbon-hydrogen bond of benzene with $Me_2Gapz(EA)Rh(CO)_2$. The monocarbonyl complex, $Me_2Gapz(EA)Rh(CO)$ was dissolved in benzene and placed in an irradiation tube. The tube was immersed in an ice bath and carbon monoxide was bubbled through the solution for one hour. The IR spectra recorded the appearance of carbonyl bands at 2095 and 2030 cm^{-1} (benzene) that were consistent with the dicarbonyl complex, $Me_2Gapz(EA)Rh(CO)_2$. The solution was irradiated for six hours by a mercury lamp. There was no change in the IR spectrum so it was concluded that no activation had taken place.

The five coordinate ethene adduct, $Me_2Gapz(EA)Rh(CO)$(ethene) (Fig. 3.3.f), was prepared by bubbling a stream of ethene through a cold benzene solution of $Me_2Gapz(EA)Rh(CO)$. In an attempt to activate a carbon hydrogen bond of benzene this solution was irradiated for several hours. No activation was observed.

3.2.4d Reactions of $Me_2Gapz(but)Rh(CO)$

The reactivity of $Me_2Gapz(but)Rh(CO)$ was tested by reaction with the same reagents. Infrared evidence suggested oxidative additions of MeI, I_2 and allyl bromide, as well as additions of carbonyl and ethene ligands had taken place. The dicarbonyl and ethene adducts were tested for C-H bond activation but no reactivity was observed. A synopsis of the reactions, with relevant IR stretches is shown in figure 3.4

3.3 Conclusions

The rhodium[I] monocarbonyl pyrazolylgallate complexes appearred to take part in oxidative additions and addition reactions but no further activity was observed.

The versatility of these ligands lies in the numerous substitutional possibilities. The subtlety of substitutions on the unsymmetrical pyrazolylgallate ligands was demonstrated by the the fact that the complex $Me_2Gapz(OCH_2CH_2NMe_2)Rh(CO)$ had shown a carbonyl insertion after oxidative addition of MeI (Fig. 3.0) where the complex $Me_2Gapz(OCH_2CH_2NH_2)Rh(CO)$ did not. The complexes differ only in that the donor nitrogen group of the bifunctional moiety on the former is methyl substituted.

Figure 3.4 Reactions of $Me_2Gapz(but)Rh(CO)$

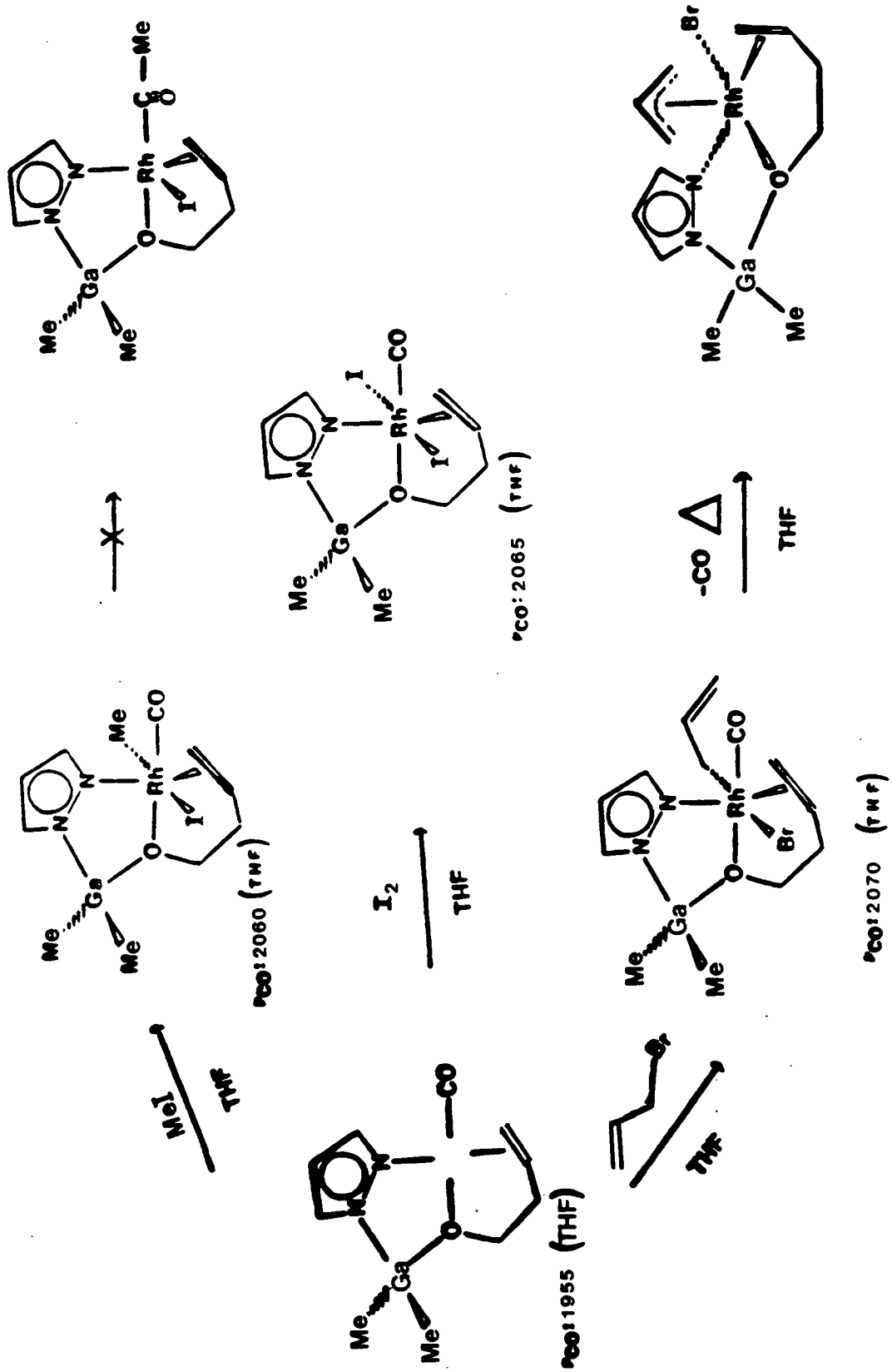

Figure 3.4 continued

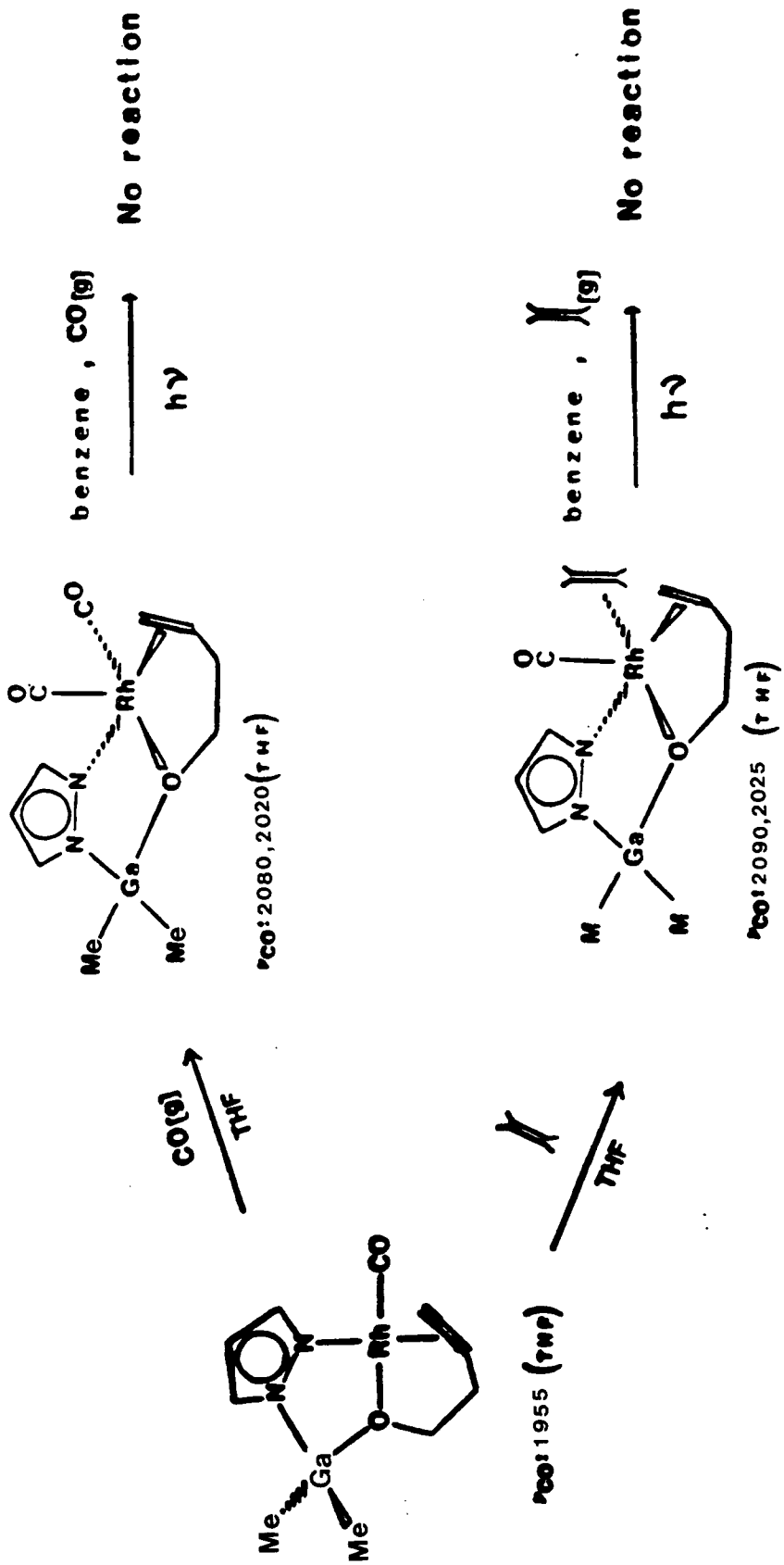

Chapter IV

Heterobimetallic Complexes Incorporating Pyrazolylborate Ligands

4.1 Introduction

It is thought that the study of simple metal-metal bonds and the cooperative effects between different metal centers in heterobimetallic complexes will lead to an understanding of higher order metal clusters, with a particular reference to catalysis[34].

In a continuing effort to form metal-metal bonds the reactions of the molybdenum anions, $[LMo(CO)_3]^-$ (L = $MeGapz_3$, $HBpz_3$, $HBpz"_3$) with a variety of transition metal halides have been carried out. Complexes with direct Mo-Rh, Mo-Cu and Mo-Sn bonds have been prepared and fully characterized[35,36,37]. This present chapter details the reactivity of $K^+[HBpz"_3Mo(CO)_3]^-$ towards $SnMe_3Cl$, $SnPh_3Cl$, the tetramer $[CuPPh_3Cl]_4$, $GePh_3Cl$ and $Ni(PPh_3)_2Cl_2$ and the results are discussed.

4.2 Experimental

The synthesis of the tridentate ligand, $K^+[HBpz"_3]^-$, is described in chapter 2. The tetramer $[CuPPh_3Cl]_4$ was prepared by a literature method[38]. $SnMe_3Cl$ was obtained from Aldrich Chemicals, $SnPh_3Cl$, $GePh_3Cl$ and $Ni(PPh_3)_2Cl_2$ were obtained from Alfa Chemicals and were used without further purification.

4.2.1 Preparation of $(MeCN)_3Mo(CO)_3$

$$Mo(CO)_6 + 3\ MeCN \xrightarrow[\text{reflux}]{} (MeCN)_3Mo(CO)_3 + 3\ CO$$

A round bottom flask was charged with 120 ml of MeCN and one gram of $Mo(CO)_6$. The colorless solution turned a yellowish-green color during a sixty hour reflux under a nitrogen atmosphere. The solvent was removed, under vacuum, leaving yellowish-green, air-sensitive crystals. It was important that the MeCN be freshly dried and distilled as the quality of the product was otherwise inferior.

The compound, $(MeCN)_3Mo(CO)_3$, has been found to be a preferred starting material for the preparation of the pyrazolyl complex anion, $[(HBpz"_3)(CO)_3Mo]^-$ [39,40]. The acetonitrile ligands are easily removed allowing almost quantitative yields of products.

The IR spectrum of $(MeCN)_3Mo(CO)_3$ showed carbonyl stretches at 1912 and 1773 cm^{-1} (THF)[41].

4.2.2 Preparation of $K^+[(HBpz"_3)Mo(CO)_3]^-$

$$K^+[HBpz"_3]^- + (MeCN)_3Mo(CO)_3 \xrightarrow[\text{reflux}]{} K^+[(HBpz"_3)(CO)_3Mo]^- + 3\ MeCN$$

A molar equivalent of $K^+[HBpz"_3]^-$ (1.22 g; 3.63 mmole), dissolved in 50 ml of THF, was added to a THF solution of $(MeCN)_3Mo(CO)_3$ (1.10 g; 3.63 mmole). The mixture was stirred overnight and a color change from light green to dark green was observed. The carbonyl stretches in the infrared spectrum shifted from 1912 and 1773 cm^{-1} (THF) to 1885,1760 and 1720 cm^{-1} (THF) signalling the completion of the reaction. The solution was then made up to a known volume with THF and stored under a nitrogen atmosphere.

4.2.3 Preparation of Heterobimetallic Complexes

4.2.3a Preparation of $(HBpz"_3)(CO)_3MoCuPPh_3$

A quarter molar equivalent of the tetramer, $[CuPPh_3Cl]_4$ (0.174 g; 0.482 mmole) dissolved in 50 ml of THF, was added to a THF solution of $K^+[(HBpz"_3)(CO)_3Mo]^-$ (1.93 mmole). The reaction mixture was stirred over night and a color change from dark green to dark brown was observed. The solvent was

removed under vacuum leaving a brown solid. This solid was redissolved in CH_2Cl_2 and the mixture was filtered. An equal portion of hexane was added and the solvent mixture allowed to evaporate slowly. Analytically pure samples were finally obtained by recrystallization from benzene.

The carbonyl stretches in the IR spectrum were seen at 1885 and 1780 cm^{-1} (Nujol).

Microanalysis: $(HBpz"_3)(CO)_3MoCuPPh_3$

Calc.	C	53.85	H	4.64	N	10.47
Found	C	54.13	H	4.85	N	10.50

4.2.3b Attempted Preparation of $(HBpz"_3)(CO)_3MoCu(PPh_2)_2CH_2$

A molar equivalent of CuI (0.168 g; 0.880 mmoles) and a molar equivalent of $Ph_2PCH_2PPh_2$ (0.336 g; 0.880 mmoles) were added to a THF solution of $K^+[(HBpz"_3)(CO)_3Mo]^-$ (0.880 mmoles). The mixture was stirred overnight. The solvent was removed under vacuum leaving a green solid. This solid was redissolved in CH_2Cl_2 and the mixture was filtered. An equal portion of hexane was added and the solvent mixture was allowed to evaporate slowly. No analytically pure samples were obtained.

4.2.3c Preparation of $(HBpz"_3)(CO)_3MoSnMe_3$

A molar equivalent of $SnMe_3Cl$ (0.332 g; 1.67 mmole), dissolved in 50 ml of THF, was added to a THF solution of $K^+[(HBpz"_3)(CO)_3Mo]^-$ (1.67 mmole). The mixture was stirred overnight and a color change from dark green to brown was observed. The solvent was removed under vacuum leaving a yellowish-brown solid. This solid was redissolved in CH_2Cl_2 and the mixture was filtered. An equal portion of hexane was added and the solvent mixture was allowed to evaporate slowly.

Microanalysis: $(HBpz"_3)(CO)_3MoSnMe_3$

Calcd.	C	39.35	H	13.11	N	4.88
Found	C	39.44	H	13.30	N	5.03

4.2.3d Preparation of $(HBpz"_3)(CO)_3MoSnPh_3$

A molar equivalent of $SnPh_3Cl$ (0.643 g; 1.67 mmole), dissolved in 50 ml of THF, was added to a THF solution of $K^+[(HBpz"_3)(CO)_3Mo]^-$ (1.67 mmole). The mixture was stirred overnight and a color change from dark green to yellow was observed. The solvent was removed under vacuum leaving a yellow solid. This solid was redissolved in CH_2Cl_2 and the mixture filtered. An equal portion of hexane was added and the solvent mixture was allowed to evaporate slowly.

The carbonyl stretches in the IR spectrum were seen at 1955 and 1865 cm^{-1} (Nujol).

Microanalysis: $(HBpz"_3)(CO)_3MoSnPh_3$

Calcd.	C	52.22	H	4.59	N	10.15
Found	C	51.85	H	4.49	N	9.95

4.2.3e Preparation of $(HBpz"_3)(CO)_3MoGePh_3$

A molar equivalent of $GePh_3Cl$ (0.101 g; 0.298 mmole), dissolved in 50 ml of THF, was added to a THF solution of $K^+[(HBpz"_3)(CO)_3Mo]^-$ (0.298 mmole). The mixture was stirred overnight and a color change from dark green to orange was observed. The solvent was removed under vacuum leaving an orange solid. This solid was redissolved in CH_2Cl_2 and the mixture was filtered. An equal portion of hexane was added and the solvent mixture was allowed to evaporate slowly.

The carbonyl stretches in the IR spectrum were seen at 2000 and 1915 cm^{-1} (THF).

Microanalysis: $(HBpz"_3)(CO)_3MoGePh_3$

Calcd.	C	55.36	H	4.78	N	10.76
Found	C	55.24	H	5.00	N	11.00

4.2.3f Attempted Preparation of

$(HBpz"_3)(CO)_3MoNi(PPh_3)_2$

A molar equivalent of $Ni(PPh_3)_2Cl_2$ (0.195 g; 0.298 mmole), dissolved in 50 ml THF, was added to a THF solution of $K^+[(HBpz"_3)(CO)_3Mo]^-$ (0.298 mmole). The mixture was stirred overnight with no apparent color change. The solvent was removed under vacuum leaving a dark green solid. This solid was redissolved in CH_2Cl_2 and the mixture was filtered. An equal portion of hexane was added and the solvent mixture was allowed to evaporate slowly. The isolated product was not identifiable by microanalysis.

The carbonyl stretches in the IR spectrum were seen at 1995,1935 and 1910 cm^{-1} (THF).

4.3 Discussion

The reactions of the transition metal anion, $[(HBpz"_3)(CO)_3Mo]^-$ with organometallic halides led to the successful synthesis of several new heterobimetallic complexes.

The reaction of $[(HBpz"_3)(CO)_3Mo]^-$ with $[CuPPh_3Cl]_4$ gave a brown compound that analysed as $(HBpz"_3)(CO)_3MoCuPPh_3$. A crystal structure of this complex was not obtained but inferences were made by the examination of the structure of an analogous compound. The compound $(MeGapz_3)(CO)_3MoCuPPh_3$ has been made and an X-ray crystal

structure has been determined[35]. The crystal structure showed that the molecule had a capped octahedral (3:3:1) geometry about the molybdenum centre with an approximate 3-fold axis along the nearly linear Ga··Mo--Cu atomic arrangement (Fig. 4.0.). The three CO ligands were essentially symmetric about this axis. The solution IR spectrum of the Cu complex showed two carbonyl bands at 1898 and 1798 cm^{-1} (CH_2Cl_2), which were consistent with a C_{3v} symmetry (*a* and *e* modes).

The X-ray data suggested there were interactions between the Cu centre and the carbonyl carbons (the Cu-C distances were 2.259(6), 2.274(7) and 2.419(6) A). The mean Mo-C-O bond angles were near linear which implied the interactions were of the semi-bridging type. The interaction

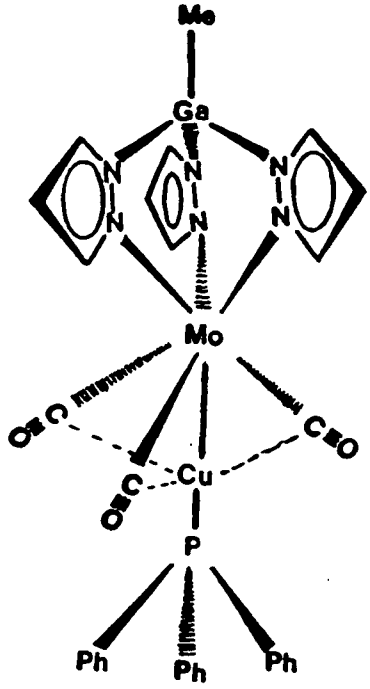

Figure 4.0 3:3:1 Structure of $(MeGapz_3)(CO)_3MoCuPPh_3$

between the Cu and Mo moieties consisted of a direct Cu-Mo bond (2.5041(8) A) and some type of semi-bridging carbonyl interaction.

The IR spectra of $(HBpz"_3)(CO)_3MoCuPPh_3$ showed two carbonyl stretches at 1885 and 1780 cm^{-1} (THF). The similarity of the spectra of $(MeGapz_3)(CO)_3MoCuPPh_3$ and $(HBpz"_3)(CO)_3MoCuPPh_3$ suggested the possibility of similar structures, that was a 3:3:1 capped octahedral structure with equivalent, semi-bridging carbonyl ligands.

The reaction of $[(HBpz"_3)(CO)_3Mo]^-$ with $SnPh_3Cl$ gave a yellow compound that analysed as $(HBpz"_3)(CO)_3MoSnPh_3$. A crystal structure was not determined but inferences were made by the examination of the X-ray crystal structure of the analogous complex, $(MeGapz_3)(CO)_3MoSnPh_3$[36]. The crystal structure showed a capped octahedral (3:3:1) geometry about the Mo centre. An approximate C_3 axis existed along the Ga··Mo--Sn atomic arrangement with the CO ligands arranged symmetrically about it. The solid state IR spectrum of this complex showed three bands (1990, 1900 and 1875 cm^{-1} (Nujol)), which were consistent with terminal carbonyls. The C-O bond lengths were within the expected range for terminal carbonyls (1.154(4), 1.139(3) and 1.141(3) A). The X-ray structure showed that one of the carbonyl groups was significantly different from the other two due to weak intermolecular hydrogen bonding. This would have brought about a departure from C_3 symmetry in the solid state and caused splitting of the *e* mode thus explaining the three

bands that were seen in the IR spectrum. The interaction between the Mo and Sn moieties consisted solely of a direct Mo-Sn bond (2.8579(3) A).

The solution IR spectrum of $(HBpz"_3)(CO)_3MoSnPh_3$ showed two carbonyl stretches at 1955 and 1865 cm^{-1} (THF). The two carbonyl bands in the IR spectra indicated a C_{3v} symmetry and the carbonyl band positions suggested terminal carbonyl ligands. A 3:3:1 capped octahedral structure with three equivalent terminal carbonyl ligands was surmised.

The reaction of $[(HBpz"_3)(CO)_3Mo]^-$ with $SnMe_3Cl$ gave a yellowish-brown compound that analysed as $(HBpz"_3)(CO)_3Mo-SnMe_3$. The Ga analog of this complex was made but an X-ray crystal structure has not been determined. The solution IR spectra of the two complexes were similar and showed three terminal carbonyls. This suggested structures similar to $(MeGapz_3)(CO)_3MoSnPh_3$.

The reaction of $[(HBpz"_3)(CO)_3Mo]^-$ with $GePh_3Cl$ gave an orange compound that analysed as $(HBpz"_3)(CO)_3MoGePh_3$. The solution IR spectrum of this compound showed two carbonyl stretches at 2000 and 1915 cm^{-1} (THF). The two carbonyl bands in the IR spectra indicated a C_{3v} symmetry and the carbonyl band positions suggested terminal carbonyl ligands. A 3:3:1 capped octahedral structure with three equivalent terminal carbonyl ligands was surmised.

4.4 Conclusion

Several new heterobimetallic complexes incorporating the pyrazolyl based molybdenum anion, $[(HBpz"_3)(CO)_3Mo]^-$ have been synthesised. Inferences about their structures have been made by comparing IR spectra with the $[(MeGapz_3)(CO)_3Mo]^-$ analogs, for which the crystal structures are known. The structures appeared to be all capped octahedral structures (3:3:1) centred about molybdenum. The Mo-Cu complex had semi-bridging interactions of the carbonyl ligands with the two metals where the Mo-Sn and Mo-Ge complexes showed only terminal carbonyl ligands.

Chapter V

Summary

The versatility of the pyrazolyl based ligand systems has been demonstrated by the three different studies presented in this thesis.

In chapter 2 the reactive pocket of a transition metal complex incorporating an intermediate, sterically hindered pyrazolylborate ligand was probed by preparing a series of compounds with less sterically hindered ligands. These mixed-ligand metal complexes were characterised by microanalysis, mass spectrometry, X-ray crystallography and electronic spectroscopy. The mass spectrometry study showed that the ligands $[HBpz_3]^-$, $[HBpz"_3]^-$ and $[MeGapz_3]^-$ formed stronger bonds to nickel and cobalt than did the sterically hindered $[HBpz^*_3]^-$ ligand. The electronic spectroscopy study showed the steric bulk of the substrate tridentate ligands determined the strength of bonding to the metal centre. The crystal structure of the four coordinate starting compound, $HBpz^*_3CoCl$ showed a trigonal pyramidal stucture. The transition energies derived from the electronic spectrum of the nickel analog, $HBpz^*_3NiCl$ compared favorably with the predicted transitions for a tetrahedral ligand field model. The crystal structure of the six coordinate complex, $HBpz^*_3Nipz"_3BH$ showed a near octahedral arrangement of the two tris-chelating pyrazolyl ligands. The crystal structure

also showed a conformational change in the bulky ligand brought about by complexation of a substrate ligand. The transition energies derived from the electronic spectrum of the nickel complex, $HBpz^{*}_{3}Nipz^{"}_{3}BH$ compared favorably with the predicted transitions for an octahedral ligand field model. The stucture of the five coordinate species was not determined and needs further study. The numerous substitutional possibilities will provide many more intermediate ligand metal complexes for future studies.

The square planar rhodium[I] complexes, $Me_2Gapz(EA)Rh(CO)$ and $Me_2Gapz(but)Rh(CO)$ underwent oxidative additions of MeI, I_2 and allyl bromide. These complexes also underwent addition reactions with ethene and carbon monoxide. The complexes were tested for C-H bond activation but no activity was observed. The subtlety of substitutions on the ligand systems and their subsequent effect on reactivity was demonstrated by comparing the oxidative addition of MeI to the complexes, $Me_2Gapz(OCH_2CH_2NH_2)Rh(CO)$ and $Me_2Gapz(OCH_2CH_2NMe_2)Rh(CO)$. The latter underwent a carbonyl insertion and differs from the former only in that the nitrogen donor group was methyl substituted. Again the substitutional possibilities on the ligand system will provide many more compounds to be tested for catalytic activity.

In the fourth chapter several new compounds were synthesized with direct metal-metal bonds. One of the metal moieties was the molybdenum anion, $[HBpz^{"}_{3}(CO)_3Mo]^{-}$,

incorporating the tridentate pyrazolylborate ligand. Reaction with transition metal halides produced complexes with Mo-Cu, Mo-Sn and Mo-Ge bonds. The structures were surmised by comparisons of IR spectra with complexes of known structures. The structures seemed to be capped octahedrons (3:3:1) about the molybdenum centre. The $HBpz"_3(CO)_3MoCuPPh_3$ complex had semi-bridging interactions of the carbonyl ligands between both metals while the complexes $HBpz"_3(CO)_3MoGePh_3$ and $HBpz"_3(CO)_3MoSnR_3$ (R = Me, Ph) had only terminal carbonyls. Future studies will most certainly involve other transition metals and substituted pyrazolyl based ligands.

References

1 S. Trofimenko, Accts. Chem. Res. 4, 17 (1971).

2 S. Trofimenko, Chem. Rev. 72, 497 (1972).

3 A. Shaver, J. Organomet. Chem. Libr. 3, 157 (1977).

4 S. Trofimenko, Inorg. Chem. 34, 115 (1986).

5 S. Trofimenko, J. Amer. Chem. Soc. 89, 6288 (1967).

6 S. Trofimenko, Inorg. Synth. 12, 99 (1970).

7 S. Trofimenko, J. Amer. Chem. Soc. 89, 3170 (1967).

8 J.C. Calabrese, S. Trofimenko and J.S. Thompson, J. Chem. Soc. Chem. Commun., 1122 (1986).

9 S. Nussbaum, S.J. Rettig, A. Storr and J. Trotter, Can. J. Chem. 63, 692 (1984).

10 B.M. Louie, S.J. Rettig, A. Storr and J. Trotter, Can. J. Chem. 62, 1057 (1984).

11 K.R. Breakell, S.J. Rettig, D.L. Singbeil, A. Storr and J. Trotter, Can. J. Chem. 56, 2099 (1978).

12 K.S. Chong, S.J. Rettig, A. Storr and J. Trotter, Can. J. Chem. 56, 1212 (1978).

13 S. Trofimenko, J.C. Calabrese and J.S. Thompson, Inorg. Chem. 26, 1507 (1987).

14 S. Trofimenko, J.C. Calabrese, P.J. Domaille and J.S. Thompson, Inorg. Chem. 28, 1091 (1989).

15 A. Storr and B.S. Thomas, Can. J. Chem. 48, 3667 (1970).

16 H. Schmidbauer and W. Findeiss, Angew. Chem. Int. Ed. 3, 696 (1964).

17 G.Dedichen, Ber. 39, 1831 (1906).

18 S. Trofimenko, J. Amer. Chem. Soc. 92, 5118 (1970).

19 D.A. Cooper, Molybdenum, Rhenium and Rhodium Complexes of Pyrazolylgallate Ligands, MSc Thesis, U.B.C. (1985).

20 M.R. Litzow and T.R. Spalding, Mass Spectrometry of Inorganic and Organometallic Compounds, American Elsevier Publishing Co. Inc., New York (1973).

21 A.B.P. Lever, Inorganic Electronic Spectroscopy (2nd Ed.), Elsevier Science Publishing Co. Inc., New York (1986).

22 M. Ciampolini, Inorg. Chem. 5, No. 1 (1965).

23 L. Sacconi, P. Paoletti and M. Ciampolini, J. Amer. Soc. 85, 411 (1963).

24 K.S. Chong, Transition Metal Derivatives of Asymmetric Pyrazolylgallate Ligands, Ph.D. Thesis, U.B.C.(1980).

25 I. Bertini, M. Ciampolini, P. Dapporto and D. Gatteschi, Inorg. Chem. 11, No. 9, 2254 (1972).

26 B.R. James, Homogeneous Hydrogenation, Wiley (1973).

27 I. Wender and P. Pino, Eds., Organic Synthesis via Metal Carbonyls, 1 (1968); 2 (1976), Wiley.

28 B. Cristensen and M.S. Scurrele, J. Chem. Soc. Faraday, 2036 (1977).

29 C.K. Gosh and W.A.G. Graham, J. Amer. Chem. Soc. 109, 4726 (1987).

30 C. Bianchini, D. Masi, A. Meli, M. Peruzzini and F. Zanobini, J. Amer. Chem. Soc. 110, 6411 (1988).

31 B.M. Louie, S.J. Rettig, A. Storr and J. Trotter, Can. J. Chem. 63, 3019 (1985).

32 E. Onyiriuka and A. Storr, Can. J. Chem. 65, 1367 (1987).

33 D.A. Cooper, S.J. Rettig and A. Storr, Can. J. Chem. 64, 566 (1986).

34 L. Carlton, W.E. Lindsell, K.J. McCullough and P.N. Preston, J. Chem. Soc. Dalton Trans. 1693 (1984).

35 G.A. Banta, B.M. Louie, E.C. Onyiriuka, S.J. Rettig and A. Storr, Can. J. Chem. 64, 373 (1986).

36 E.C. Onyiriuka, S.J. Rettig and A Storr, Can. J. Chem. 64, 321 (1986).

37 Y.Y. Liu, A.Mar, S.J. Rettig, A Storr and J. Trotter, Can. J. Chem 66, 1997 (1988).

38 G. Costa, E. Reisenhofer and L. Stefani, J. Inorg. Nucl. Chem. 27, 2581 (1965).

39 F.A. Cotton, Inorg. Chem. 3, 702 (1964).

40 K.F. Purcell and J.C. Kotz, Inorganic Chemistry, W.B. Saunders Company, Philidelphia (1977).

41 E.C. Onyiriuka, Pyrazolyl Ligands in Mixed Metal Complexes, Ph. D. Thesis, U.B.C. (1986).

42 L. Carlton, W.E. Lindsell, K.J. McCullough and P.N. Preston, Organomet. 4, 1138 (1985).

43 J.A. Riddick and W.B. Burger, Organic Solvents, Physical Properties and Methods of Purification, 3rd ed., Techniques of Chemistry Vol. II, Wiley (1970).

Appendix 1

Crystal Grower

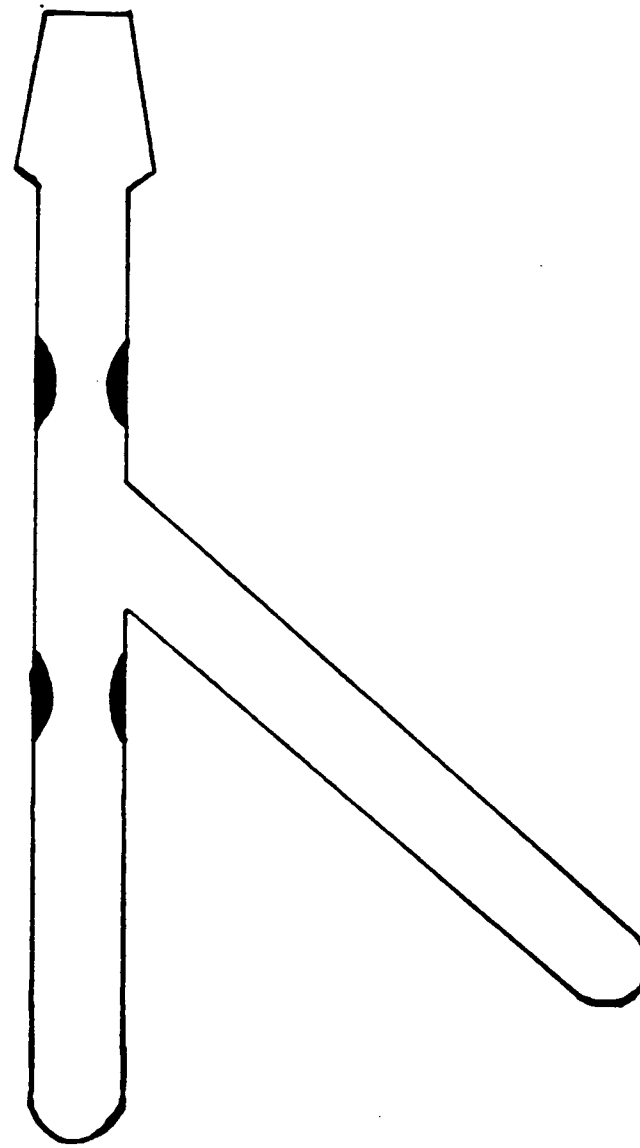

Appendix 2

Isotopic Clusters of B, Ga Br and Cl

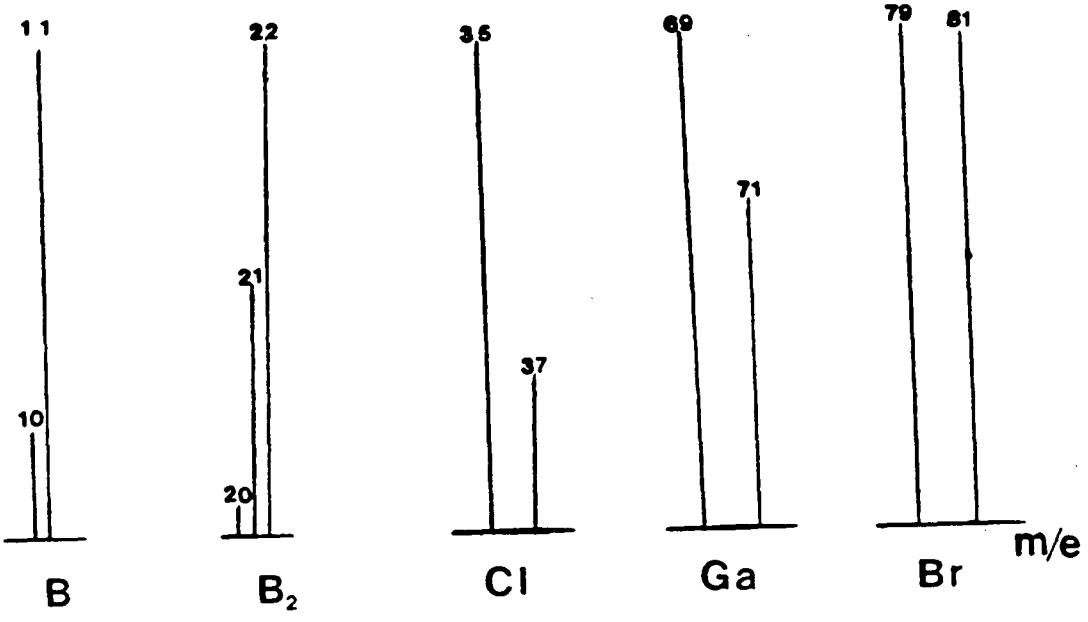

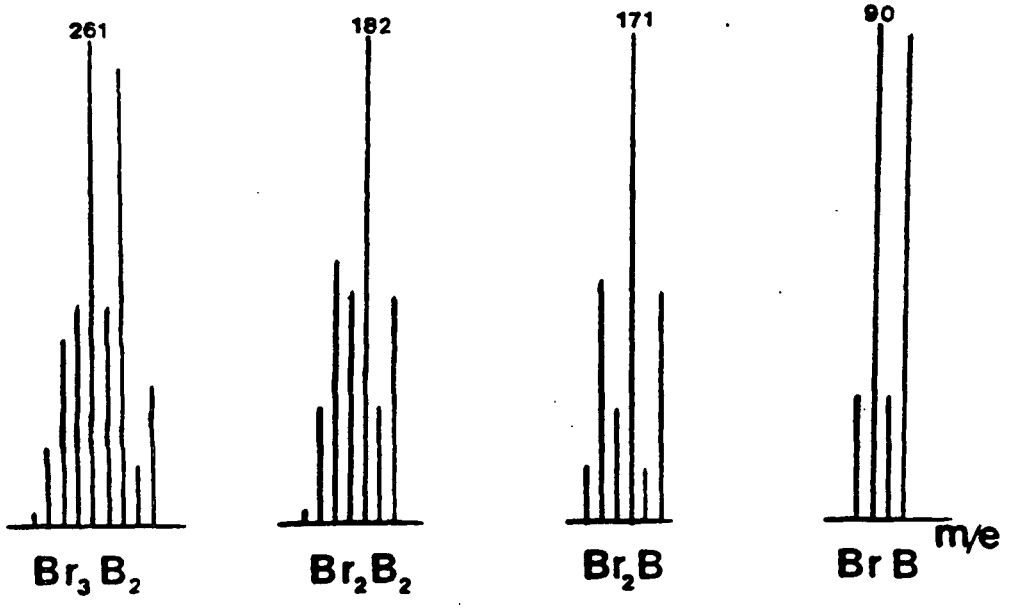

Isotopic Clusters of B, Ga Br and Cl

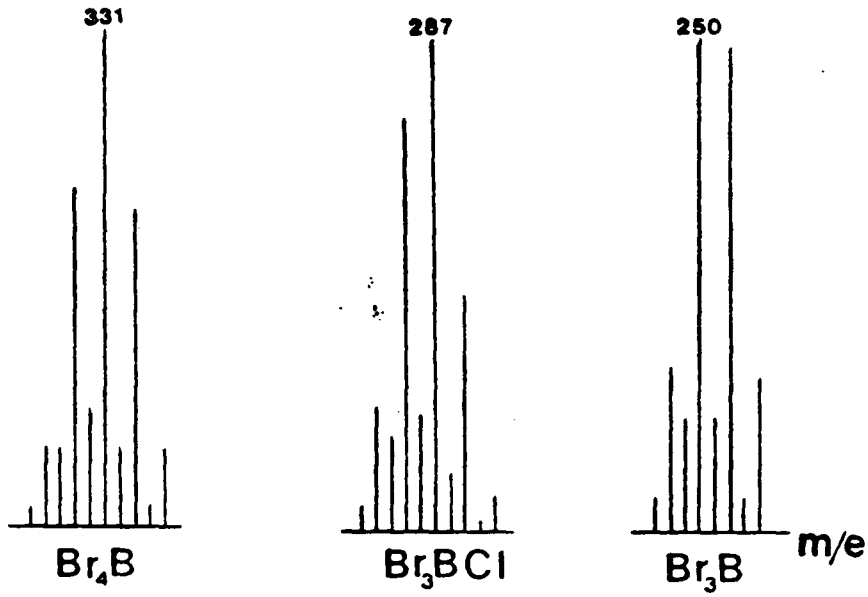

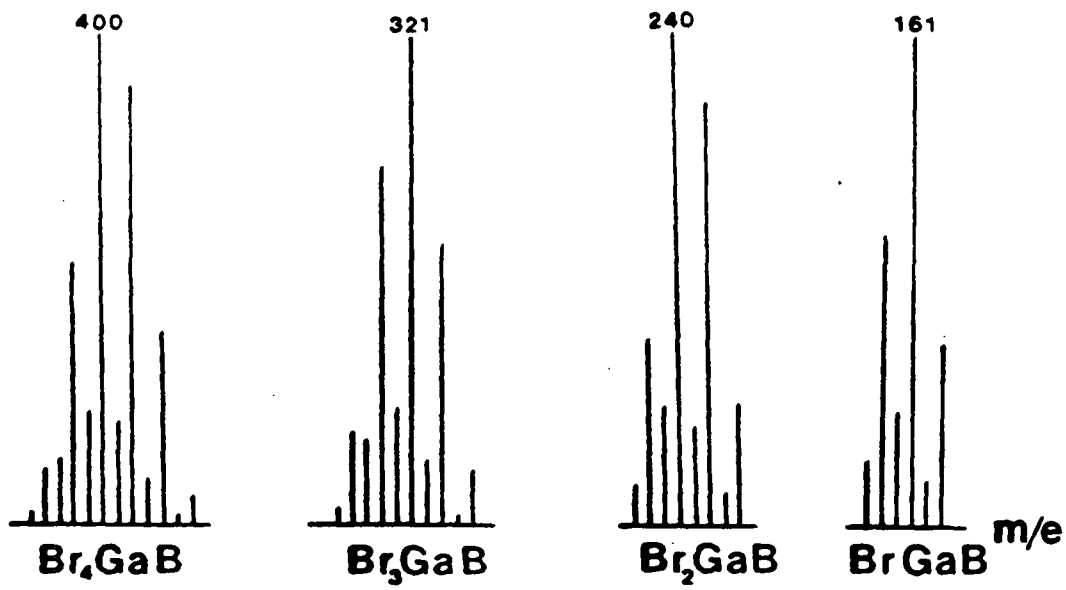

Appendix 3.a

X-ray Structural Data of $HBpz^*_3CoCl$

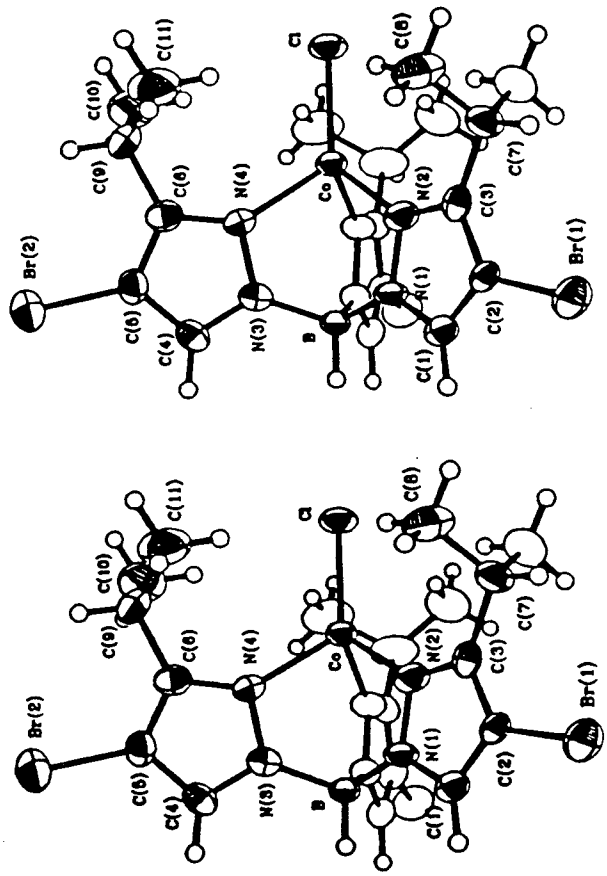

Bond lengths (Å) with estimated standard deviations in parentheses

Bond	Length(A)	Bond	Length(A)
Br(1)-C(2)	1.874(10)	N(3)-B	1.540(8)
Br(2)-C(5)	1.876(7)	N(4)-C(6)	1.347(9)
Co -Cl	2.207(3)	C(1)-C(2)	1.352(15)
Co -N(2)	2.057(9)	C(2)-C(3)	1.397(13)
Co -N(4)	2.039(6)	C(3)-C(7)	1.52(2)
N(1)-N(2)	1.385(11)	C(4)-C(5)	1.360(10)
N(1)-C(1)	1.358(12)	C(5)-C(6)	1.381(11)
N(1)-B	1.514(13)	C(6)-C(9)	1.510(10)
N(2)-C(3)	1.309(13)	C(7)-C(8)	1.513(11)
N(3)-N(4)	1.383(8)	C(9)-C(10)	1.544(14)
N(3)-C(4)	1.332(8)	C(9)-C(11)	1.525(15)

Bond angles (deg) with estimated standard deviations in parentheses

Bonds	Angle(deg)	Bonds	Angle(deg)
Cl -Co -N(2)	122.7(3)	C(1)-C(2)-C(3)	106.8(9)
Cl -Co -N(4)	121.8(2)	N(2)-C(3)-C(2)	108.9(9)
Cl -Co -N(4)'	121.8(2)	N(2)-C(3)-C(7)	122.8(9)
N(2)-Co -N(4)	94.1(2)	C(2)-C(3)-C(7)	128.3(9)
N(2)-Co -N(4)'	94.1(2)	N(3)-C(4)-C(5)	108.3(6)
N(4)-Co -N(4)'	94.9(3)	Br(2)-C(5)-C(4)	126.5(6)
N(2)-N(1)-C(1)	107.5(9)	Br(2)-C(5)-C(6)	126.3(5)
N(2)-N(1)-B	121.9(7)	C(4)-C(5)-C(6)	107.2(6)
C(1)-N(1)-B	130.6(9)	N(4)-C(6)-C(5)	108.7(6)
Co -N(2)-N(1)	109.3(6)	N(4)-C(6)-C(9)	122.7(7)
Co -N(2)-C(3)	142.3(7)	C(5)-C(6)-C(9)	128.6(7)
N(1)-N(2)-C(3)	108.4(8)	C(3)-C(7)-C(8)	111.6(6)
N(4)-N(3)-C(4)	109.3(5)	C(3)-C(7)-C(8)'	111.6(6)
N(4)-N(3)-B	120.5(6)	C(8)-C(7)-C(8)'	110.9(10)
C(4)-N(3)-B	130.2(6)	C(6)-C(9)-C(10)	109.8(8)
Co -N(4)-N(3)	110.6(4)	C(6)-C(9)-C(11)	112.7(8)
Co -N(4)-C(6)	142.8(5)	C(10)-C(9)-C(11)	110.9(8)
N(3)-N(4)-C(6)	106.5(6)	N(1)-B -N(3)	110.2(5)
N(1)-C(1)-C(2)	108.4(9)	N(1)-B -N(3)'	110.2(5)
Br(1)-C(2)-C(1)	125.9(7)	N(3)-B -N(3)'	109.2(7)
Br(1)-C(2)-C(3)	127.3(8)		

Final positional (fractional x 10^4; Br, Co, Cl x 10^5) and isotropic thermal parameters (U x 10^3 A^2) with estimated standard deviations in parentheses

Atom	x	y	z	U_{eq}
Br(1)	0	56130(10)	33034	45
Br(2)	32108(5)	-2959(9)	-27(10)	57
Co	0	1747(13)	24225(13)	30
Cl	0	-11245(23)	35014(18)	43
N(1)	0	2622(7)	1794(5)	32
N(2)	0	2056(8)	2583(6)	37
N(3)	861(4)	1070(5)	927(4)	33
N(4)	1031(4)	196(5)	1546(4)	36
C(1)	0	3858(9)	1927(7)	33
C(2)	0	4065(8)	2774(7)	26
C(3)	0	2912(8)	3169(7)	32
C(4)	1535(5)	1046(7)	355(5)	35
C(5)	2138(5)	148(7)	581(5)	35
C(6)	1821(5)	-365(7)	1328(5)	37
C(7)	0	2621(10)	4115(8)	44
C(8)	855(7)	1926(8)	4375(5)	59
C(9)	2249(6)	-1374(8)	1857(6)	61
C(10)	1623(8)	-2522(8)	1852(7)	78
C(11)	2455(7)	-964(11)	2765(7)	76
B	0	1889(9)	975(7)	29

Appendix 3.b

X-ray Structural Data of $HBpz^{*}_{3}Copz^{"}BH$

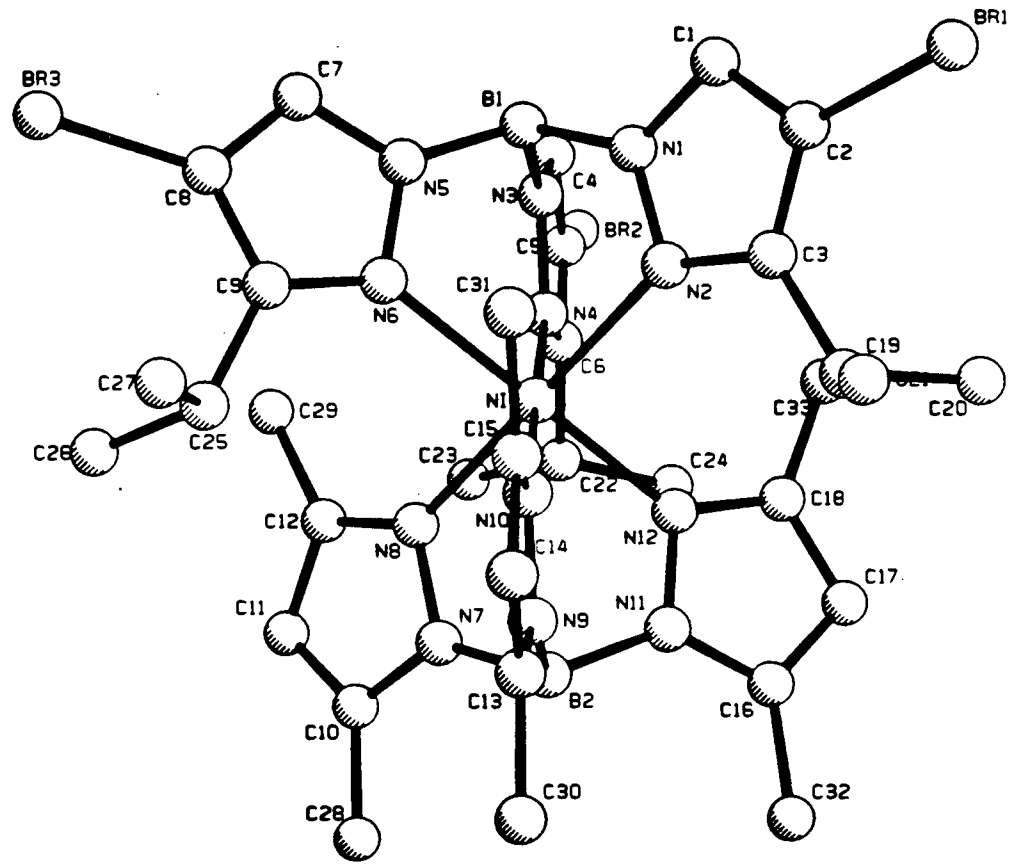

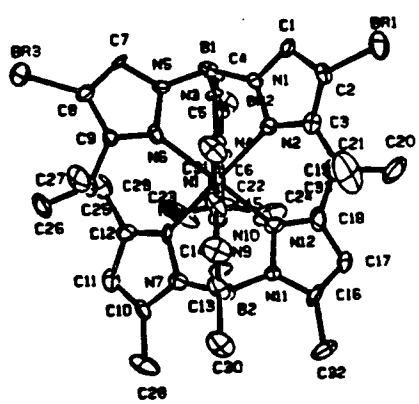

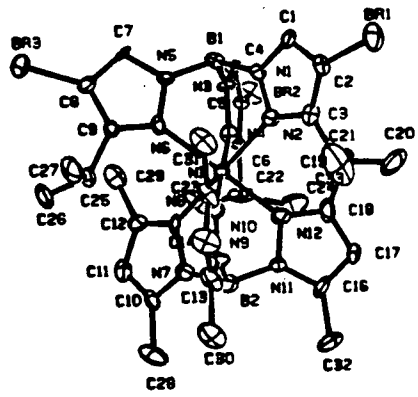

Empirical Formula	C(33)H(47)B(2)Br(3)N(12)Ni(1)
Formula Weight	931.85
Crystal System	Orthorhombic
Lattice Parameters:	a = 20.65 (1) angstroms b = 29.158 (3) angstroms c = 13.306 (2) angstroms V = 8011 (4) angstroms**3
Space Group	Pbca (#61)
Z value	8
Dcalc	1.55 g/cm**3
F000	3776
mu(Mo K-alpha)	34.90 cm**-1
Diffractometer	Rigaku AFC6
Radiation	Mo K-alpha (lambda= 0.71069) Graphite-monochromated
Temperature	21 degrees Cent.
2-theta(max)	50.0 degrees
No. Observations (I>2.00(sig(I)))	1976
No. Variables	460
Residuals: R; Rw	0.054; 0.048
Goodness of Fit Indicator	1.37
Maximum Shift in Final Cycle	0.09
Largest Peak in Final Diff. Map	0.50 e/angstrom**3

Intramolecular Distances Involving the Nonhydrogen Atoms

atom	atom	distance	atom	atom	distance
Br(1)	C(2)	1.89(1)	N(9)	N(10)	1.37(2)
Br(2)	C(5)	1.90(1)	N(9)	B(2)	1.49(2)
Br(3)	C(8)	1.86(1)	N(10)	C(15)	1.33(2)
Ni	N(12)	2.05(1)	N(11)	C(16)	1.34(2)
Ni	N(8)	2.07(1)	N(11)	N(12)	1.36(1)
Ni	N(10)	2.08(1)	N(11)	B(2)	1.54(2)
Ni	N(4)	2.13(1)	N(12)	C(18)	1.34(2)
Ni	N(2)	2.15(1)	C(1)	C(2)	1.35(2)
Ni	N(6)	2.16(1)	C(2)	C(3)	1.39(2)
N(1)	N(2)	1.35(1)	C(3)	C(19)	1.52(2)
N(1)	C(1)	1.35(1)	C(4)	C(5)	1.35(2)
N(1)	B(1)	1.53(2)	C(5)	C(6)	1.35(2)
N(2)	C(3)	1.34(2)	C(6)	C(22)	1.51(2)
N(3)	C(4)	1.32(1)	C(7)	C(8)	1.37(2)
N(3)	N(4)	1.37(1)	C(8)	C(9)	1.39(2)
N(3)	B(1)	1.54(2)	C(9)	C(25)	1.55(2)
N(4)	C(6)	1.38(2)	C(10)	C(11)	1.33(2)
N(5)	C(7)	1.34(1)	C(10)	C(28)	1.51(2)
N(5)	N(6)	1.38(1)	C(11)	C(12)	1.41(2)
N(5)	B(1)	1.51(2)	C(12)	C(29)	1.52(2)
N(6)	C(9)	1.32(2)	C(13)	C(14)	1.34(2)
N(7)	C(10)	1.35(2)	C(13)	C(30)	1.49(2)
N(7)	N(8)	1.37(1)	C(14)	C(15)	1.42(2)
N(7)	B(2)	1.53(2)	C(15)	C(31)	1.50(2)
N(8)	C(12)	1.30(2)	C(16)	C(17)	1.35(2)
N(9)	C(13)	1.36(2)	C(16)	C(32)	1.52(2)

Distances are in angstroms. Estimated standard deviations in the least significant figure are given in parentheses.

atom	atom	distance	atom	atom	distance
C(17)	C(18)	1.38(2)			
C(18)	C(33)	1.51(2)			
C(19)	C(21)	1.52(2)			
C(19)	C(20)	1.54(2)			
C(22)	C(23)	1.50(2)			
C(22)	C(24)	1.56(2)			
C(25)	C(26)	1.51(2)			
C(25)	C(27)	1.53(2)			

Distances are in angstroms. Estimated standard deviations in the least significant figure are given in parentheses.

atom	atom	atom	angle	atom	atom	atom	angle
N(12)	Ni	N(8)	88.3(5)	C(6)	N(4)	Ni	140(1)
N(12)	Ni	N(10)	89.7(5)	C(7)	N(5)	N(6)	108(1)
N(12)	Ni	N(4)	89.8(5)	C(7)	N(5)	B(1)	130(1)
N(12)	Ni	N(2)	91.6(5)	N(6)	N(5)	B(1)	122(1)
N(12)	Ni	N(6)	179.2(4)	C(9)	N(6)	N(5)	107(1)
N(8)	Ni	N(10)	88.7(5)	C(9)	N(6)	Ni	140(1)
N(8)	Ni	N(4)	91.8(5)	N(5)	N(6)	Ni	113(1)
N(8)	Ni	N(2)	179.7(7)	C(10)	N(7)	N(8)	109(1)
N(8)	Ni	N(6)	91.1(5)	C(10)	N(7)	B(2)	134(1)
N(10)	Ni	N(4)	179.3(5)	N(8)	N(7)	B(2)	117(1)
N(10)	Ni	N(2)	91.0(5)	C(12)	N(8)	N(7)	107(1)
N(10)	Ni	N(6)	90.8(5)	C(12)	N(8)	Ni	136(1)
N(4)	Ni	N(2)	88.4(5)	N(7)	N(8)	Ni	117(1)
N(4)	Ni	N(6)	89.7(4)	C(13)	N(9)	N(10)	107(1)
N(2)	Ni	N(6)	88.9(5)	C(13)	N(9)	B(2)	134(2)
N(2)	N(1)	C(1)	111(1)	N(10)	N(9)	B(2)	119(1)
N(2)	N(1)	B(1)	123(1)	C(15)	N(10)	N(9)	110(1)
C(1)	N(1)	B(1)	127(1)	C(15)	N(10)	Ni	135(1)
C(3)	N(2)	N(1)	107(1)	N(9)	N(10)	Ni	115(1)
C(3)	N(2)	Ni	141(1)	C(16)	N(11)	N(12)	110(1)
N(1)	N(2)	Ni	112.8(8)	C(16)	N(11)	B(2)	132(2)
C(4)	N(3)	N(4)	111(1)	N(12)	N(11)	B(2)	117(1)
C(4)	N(3)	B(1)	129(1)	C(18)	N(12)	N(11)	105(1)
N(4)	N(3)	B(1)	120(1)	C(18)	N(12)	Ni	137(1)
N(3)	N(4)	C(6)	105(1)	N(11)	N(12)	Ni	117(1)
N(3)	N(4)	Ni	115(1)	C(2)	C(1)	N(1)	107(1)

Angles are in degrees. Estimated standard deviations in the least significant figure are given in parentheses.

atom	atom	atom	angle	atom	atom	atom	angle
C(1)	C(2)	C(3)	107(1)	C(11)	C(12)	C(29)	126(2)
C(1)	C(2)	Br(1)	125(1)	C(14)	C(13)	N(9)	109(2)
C(3)	C(2)	Br(1)	128(1)	C(14)	C(13)	C(30)	130(2)
N(2)	C(3)	C(2)	109(1)	N(9)	C(13)	C(30)	121(2)
N(2)	C(3)	C(19)	121(1)	C(13)	C(14)	C(15)	107(1)
C(2)	C(3)	C(19)	130(1)	N(10)	C(15)	C(14)	106(2)
N(3)	C(4)	C(5)	108(1)	N(10)	C(15)	C(31)	125(2)
C(6)	C(5)	C(4)	108(1)	C(14)	C(15)	C(31)	129(2)
C(6)	C(5)	Br(2)	129(1)	N(11)	C(16)	C(17)	109(2)
C(4)	C(5)	Br(2)	123(1)	N(11)	C(16)	C(32)	123(2)
C(5)	C(6)	N(4)	108(1)	C(17)	C(16)	C(32)	129(2)
C(5)	C(6)	C(22)	129(1)	C(16)	C(17)	C(18)	105(1)
N(4)	C(6)	C(22)	122(1)	N(12)	C(18)	C(17)	111(2)
N(5)	C(7)	C(8)	109(1)	N(12)	C(18)	C(33)	122(2)
C(7)	C(8)	C(9)	105(1)	C(17)	C(18)	C(33)	128(2)
C(7)	C(8)	Br(3)	124(1)	C(3)	C(19)	C(21)	113(2)
C(9)	C(8)	Br(3)	131(1)	C(3)	C(19)	C(20)	112(2)
N(6)	C(9)	C(8)	110(1)	C(21)	C(19)	C(20)	107(1)
N(6)	C(9)	C(25)	124(2)	C(23)	C(22)	C(6)	113(1)
C(8)	C(9)	C(25)	126(1)	C(23)	C(22)	C(24)	108(1)
C(11)	C(10)	N(7)	108(1)	C(6)	C(22)	C(24)	111(1)
C(11)	C(10)	C(28)	131(1)	C(26)	C(25)	C(27)	111(1)
N(7)	C(10)	C(28)	121(1)	C(26)	C(25)	C(9)	113(1)
C(10)	C(11)	C(12)	106(1)	C(27)	C(25)	C(9)	110(1)
N(8)	C(12)	C(11)	109(1)	N(5)	B(1)	N(1)	110(1)
N(8)	C(12)	C(29)	125(1)	N(5)	B(1)	N(3)	110(1)

Angles are in degrees. Estimated standard deviations in the least significant figure are given in parentheses.

atom	atom	atom	angle	atom	atom	atom	angle
N(1)	B(1)	N(3)	109(1)				
N(9)	B(2)	N(7)	111(1)				
N(9)	B(2)	N(11)	110(1)				
N(7)	B(2)	N(11)	110(1)				

Angles are in degrees. Estimated standard deviations in the least significant figure are given in parentheses.